Light Scattering by a Spheroidal Particle

Shoji Asano and Giichi Yamamoto

The solution of electromagnetic scattering by a homogeneous prolate (or oblate) spheroidal particle with an arbitrary size and refractive index is obtained for any angle of incidence by solving Maxwell's equations under given boundary conditions. The method used is that of separating the vector wave equations in the spheroidal coordinates and expanding them in terms of the spheroidal wavefunctions. The unknown coefficients for the expansion are determined by a system of equations derived from the boundary conditions regarding the continuity of tangential components of the electric and magnetic vectors across the surface of the spheroid. The solutions both in the prolate and oblate spheroidal coordinate systems result in a same form, and the equations for the oblate spheroidal system can be obtained from those for the prolate one by replacing the prolate spheroidal wavefunctions with the oblate ones and vice versa. For an oblique incidence, the polarized incident wave is resolved into two components, the TM mode for which the magnetic vector vibrates perpendicularly to the incident plane and the TE mode for which the electric vector vibrates perpendicularly to this plane. For the incidence along the rotation axis the resultant equations are given in the form similar to the one for a sphere given by the Mie theory. The physical parameters involved are the following five quantities: the size parameter defined by the product of the semifocal distance of the spheroid and the propagation constant of the incident wave, the eccentricity, the refractive index of the spheroid relative to the surrounding medium, the incident angle between the direction of the incident wave and the rotation axis, and the angles that specify the direction of the scattered wave.

I. Introduction

The scattering theory for a homogeneous sphere with arbitrary size was developed by Mie[1] and the scattering by an infinitely long circular cylinder was solved by Lord Rayleigh[2] at normal incidence and by Wait[3] at oblique incidence. Since then the solutions for spheres and cylinders have been rederived and calculated by many investigators. For an ellipsoidal particle, the exact solution may be, in principle, obtained by means of the method of separation of variables. Möglish[4] has attempted to formulate the problem of scattering by an ellipsoid in the ellipsoidal coordinate system and to express the Hertz vectors of the scattered and internal fields in series of ellipsoidal harmonics. His solution is a purely formal one. The radar cross section of a perfectly conducting prolate spheroid with nose-on incidence has been solved by Schultz,[5] and some numerical calculations have been carried out by Siegel *et al.*[6]

In this paper, the scattering theory of the linearly polarized electromagnetic wave by a homogeneous prolate (or oblate) spheroid with any size and refractive index has been studied. The approach is to separate the vector wave equation in the spheroidal coordinates, which have been chosen in such a way that the surface of the particle coincides with one of the coordinate surfaces. Then the solution of the wave equation is expanded in terms of the spheroidal wavefunctions, and the expansion coefficients are determined under the boundary conditions.

The authors are with the Geophysical Institute, Tohoku University, Katahira-2 chome, Sendai, Japan.

Received 14 September 1973.

II. General Theory of Electromagnetic Scattering

We consider the scattering of a plane, linearly polarized monochromatic wave by a homogeneous spheroidal particle, which is prolate or oblate, immersed in a homogeneous, isotropic medium. It is assumed that the medium in which the scattering spheroid is embedded is a nonconductor and that both the medium and the spheroid are nonmagnetic.

If we assume the time-dependent part of the electromagnetic field to be $\exp(-i\omega t)$, the time-independent parts of the electric and magnetic field vectors both outside and inside the spheroid satisfy Maxwell's equations in their time-free form[7,8]

$$\left.\begin{aligned} \nabla \times \mathbf{E} &= ik_0 \mathbf{H}, \\ \nabla \times \mathbf{H} &= -ik_0 \mathcal{K}^2 \mathbf{E}, \end{aligned}\right\} \tag{1}$$

or the vector wave equations

$$\left.\begin{aligned} \nabla^2 \mathbf{E} + k^2 \mathbf{E} &= 0, \\ \nabla^2 \mathbf{H} + k^2 \mathbf{H} &= 0, \end{aligned}\right\} \tag{2}$$

where

$$k_0 = \omega/c = 2\pi/\lambda_0, \tag{3}$$

$$\mathfrak{C} = \epsilon\mu + i\,(4\pi\sigma\mu/\omega), \tag{4}$$

and

$$k = k_0\mathfrak{C}. \tag{5}$$

Both k_0 and $\mathfrak{C}$ are important parameters: k_0 is the propagation constant (or wavenumber) in vacuum and the wavelength in vacuum λ_0 follows from it by $\lambda_0 = 2\pi/k_0$, and $\mathfrak{C}$ is the complex refractive index of the medium at the circular frequency ω. The parameter k given by Eq. (5) is the propagation constant in the medium with refractive index $\mathfrak{C}$.

The quantities that refer to the surrounding medium will be denoted by superscript I, and those referring to the spheroid by II. From the assumption, we have $\sigma^{(I)} = 0$ and $\mu^{(I)} = \mu^{(II)} = 1$.

As regards the boundary conditions, it is only demanded that the tangential components of **E** and **H** be continuous across the surface of the spheroid. The condition that the normal components of ϵ**E** and **H** be continuous across the surface follows from the above conditions and from Maxwell's equations. In order to satisfy the boundary conditions, it must be assumed that apart from the incident field $^{(i)}$**E**, $^{(i)}$**H**, and the field $^{(t)}$**E**, $^{(t)}$**H** within the spheroid, there is a secondary scattered field $^{(s)}$**E**, $^{(s)}$**H** in the ambient medium. Since the boundary conditions must hold for all time, all six field vectors must have the same time dependence $\exp(-i\omega t)$, which will be omitted in the sequences.

III Wavefunctions in the Spheroidal Coordinate System

The spheroidal coordinates are obtained by rotation of an ellipse about an axis of symmetry. Two cases are to be distinguished, according to whether the rotation takes place about the major axis (prolate spheroid) or about the minor axis (oblate spheroid). It is customary to make the z axis the axis of revolution in each case. We shall denote the semifocal distance by l.

The prolate and oblate spheroidal coordinate systems (η,ξ,ϕ), where η is an angular coordinate, ξ is a radial one, and ϕ is an azimuthal one, as shown in Fig. 1 taking the prolate spheroidal coordinate system as an example, are related to the Cartesian system (x,y,z) by the transformation

$$\begin{aligned} x &= l(1-\eta^2)^{1/2}(\xi^2 \mp 1)^{1/2}\cos\phi, \\ y &= l(1-\eta^2)^{1/2}(\xi^2 \mp 1)^{1/2}\sin\phi,\ z = l\eta\xi, \end{aligned} \tag{6}$$

with

$$-1 \le \eta \le 1, \quad 1 \le \xi < \infty, \quad 0 \le \phi \le 2\pi \tag{7}$$

for the prolate system and with

$$-1 \le \eta \le 1, \quad 0 \le \xi < \infty, \quad 0 \le \phi \le 2\pi \tag{8}$$

for the oblate one. In all pairs of signs in Eqs. (6) and in the following expressions, the upper sign corresponds to the prolate spheroidal system and the lower one to the oblate system.

The size and shape of the ellipse are specified by such two quantities as the semifocal distance l and the eccentricity, and it must be remembered that the eccentricity e is related to the radial coordinate ξ as

$$e = 1/\xi_0 \tag{9}$$

in the prolate system and as

$$e = 1/(\xi_0^2 + 1)^{1/2} \tag{10}$$

in the oblate one, respectively, where ξ_0 is the value of ξ on the surface of the spheroid in each system.

It is worth noting that in the limit when the semifocal distance l becomes zero, both the prolate and oblate spheroidal systems reduce to the spherical coordinate system and that, for l finite, the surface ξ = constant in each case becomes spherical as ξ approaches infinity; thus

$$l\xi \longrightarrow r,\ \eta \longrightarrow \cos\theta,\ \text{as}\ \xi \longrightarrow \infty, \tag{11}$$

where r and θ are the usual spherical coordinates. Furthermore, as the eccentricity of the ellipse approaches unity the prolate spheroid becomes rod-shaped, whereas the oblate spheroid degenerates into a flat, circular disk. The practical utility of the spheroidal coordinates may be surmised from those facts.

Solutions of the vector wave Eq. (2) are to be formed from solutions of the scalar wave equation by means of the procedure set forth by Stratton.[7]

The scalar wave equation

$$\nabla^2\psi + k^2\psi = 0 \tag{12}$$

is separable in the spheroidal coordinate system, and three second-order linear ordinary differential equations result, one in η, one in ξ, and one in ϕ. The solutions of Eq. (12) in the spheroidal coordinate sys-

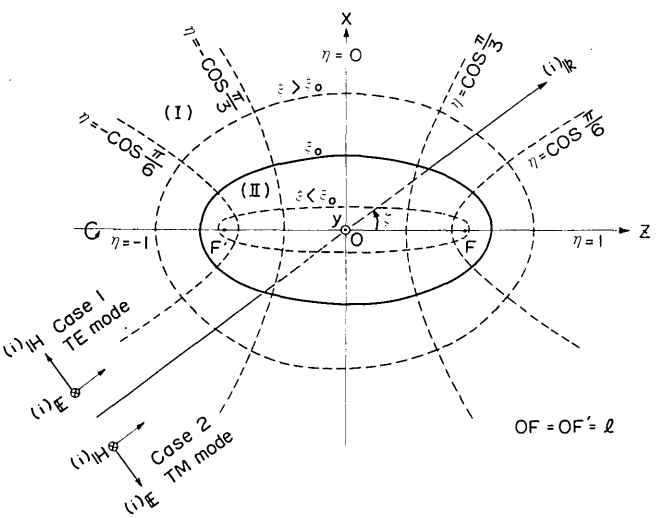

Fig. 1. Coordinate system for scattering by a prolate spheroid with semifocal distance l. The prolate spheroidal coordinates are η,ξ,ϕ. The z axis is chosen as the axis of revolution. The incident plane contains the incident direction and the z axis. The x axis is in the incident plane; for the TM mode, **E** is in the incident plane; for the TE mode, **H** is in the incident plane. The incident angle ζ is the angle in the incident plane between the incident direction and the z axis.

tem are the scalar spheroidal wavefunctions. For the sake of completeness and to facilitate the explanation of notation, we shall, in this section, briefly review some basic properties of the spheroidal wavefunctions mainly according to the comprehensive text by Flammer.[9]

The solutions of the equation in ϕ are $e^{im\phi}$, $\cos m\phi$, and $\sin m\phi$. Obviously, in the present work, the separation constant m must be an integer, which we can restrict to positive or zero values ($m = 0,1,2, \ldots$).

For the equation in η,

$$\frac{d}{d\eta}\left[(1-\eta^2)\frac{dS_{mn}(\eta)}{d\eta}\right] + \left(\lambda_{mn} \mp c^2\eta^2 - \frac{m^2}{1-\eta^2}\right)S_{mn}(\eta) = 0, \tag{13}$$

where

$$c = l \cdot k, \tag{14}$$

and $S_{mn}(\eta)$ is the spheroidal angular function of order m and degree n, and the solutions of the first kind are used, since only these solutions are regular throughout the range of $\eta(-1 \leq \eta \leq 1)$. In Eq. (13) λ_{mn} is a separation constant, which is a function of c defined by Eq. (14). Those discrete values of $\lambda_{mn}(c)$ ($n = m, m+1, m+2, \ldots$), for which the differential equation admits finite solutions at $\eta = \pm 1$, are the desired eigenvalues. The eigenvalues $\lambda_{mn}(c)$ and the associated eigenfunctions $S_{mn}(c;\eta)$ correspond to the prolate system. Replacement of c by $-ic$ leads to the oblate spheroidal eigenvalues $\lambda_{mn}(-ic)$ and angle functions of the first kind $S_{mn}(-ic;\eta)$, where and hereafter $i = (-1)^{1/2}$. The prolate and oblate angle functions can be, respectively, expressed in such infinite series of the associated Legendre functions of the first kind as

$$S_{mn}(c;\eta) = \sum_{r=0,1}^{\infty}{}' d_r^{mn}(c) P_{m+r}^{m}(\eta), \tag{15}$$

and

$$S_{mn}(-ic;\eta) = \sum_{r=0,1}^{\infty}{}' d_r^{mn}(-ic) P_{m+r}^{m}(\eta), \tag{16}$$

where $d_r^{mn}(c)$ and $d_r^{mn}(-ic)$ are the expansion coefficients relating to the prolate and oblate coordinate systems, respectively. The prime over the summation symbols indicates that the summation is over (only) even values when $n - m$ is even and over (only) odd values when $n - m$ is odd. Thus, the spheroidal angle functions depend not only on the angular component but also on the characteristics of the medium c. In the spherical geometry, however, the angle functions reduce to $P_n^m(\eta)$, which are not dependent on c.

From the theory of Sturm-Liouville differential equations, it follows that the angle functions $S_{mn}(\eta)$ form an orthogonal set on the interval $-1 \leq \eta \leq 1$. Thus,

$$\int_{-1}^{+1} S_{mn}(\eta) S_{mn'}(\eta) d\eta = \begin{cases} 0 & (n \neq n') \\ \Lambda_{mn} & (n = n') \end{cases}, \tag{17}$$

where Λ_{mn} is the normalization constant and given by

$$\Lambda_{mn} = \sum_{r=0,1}^{\infty}{}' \frac{2\cdot(r+2m)!}{(2r+2m+1)\cdot r!}\left(d_r^{mn}\right)^2. \tag{18}$$

The radial functions $R_{mn}(\xi)$, which satisfy the differential equations

$$\frac{d}{d\xi}\left[(\xi^2 \mp 1)\frac{dR_{mn}(\xi)}{d\xi}\right] - \left[\lambda_{mn} - c^2\xi^2 \pm \frac{m^2}{(\xi^2 \mp 1)}\right]R_{mn}(\xi) = 0, \tag{19}$$

are normalized such that, for $c\xi \to \infty$, they have the asymptotic forms

$$R_{mn}^{(1)} \longrightarrow \frac{1}{c\xi}\cos\left(c\xi - \frac{n+1}{2}\pi\right), \tag{20}$$

$$R_{mn}^{(2)} \longrightarrow \frac{1}{c\xi}\sin\left(c\xi - \frac{n+1}{2}\pi\right), \tag{21}$$

$$R_{mn}^{(3)} \longrightarrow \frac{1}{c\xi}\exp\left[i\left(c\xi - \frac{n+1}{2}\pi\right)\right], \tag{22}$$

$$R_{mn}^{(4)} \longrightarrow \frac{1}{c\xi}\exp\left[-i\left(c\xi - \frac{n+1}{2}\pi\right)\right], \tag{23}$$

where the superscripts indicate which of the four kinds are being referred to. The appropriate expansions in terms of the spherical Bessel functions are

$$R_{mn}^{(j)}(c;\xi) = \left\{1/\left[\sum_{r=0,1}{}' \frac{(r+2m)!}{r!} d_r^{mn}(c)\right]\right\}\left[\frac{\xi^2-1}{\xi^2}\right]^{m/2} \cdot \sum_{r=0,1}{}' i^{r+n-m} d_r^{mn}(c) \frac{(r+2m)!}{r!} z_{m+r}^{(j)}(c\xi) \tag{24}$$

for the prolate radial functions and

$$R_{mn}^{(j)}(-ic;i\xi) = \left\{1/\left[\sum_{r=0,1}{}' \frac{(r+2m)!}{r!} d_r^{mn}(-ic)\right]\right\} \times \left[\frac{\xi^2+1}{\xi^2}\right]^{m/2} \sum_{r=0,1}{}' i^{r+n-m} d_r^{mn}(-ic) \frac{(r+2m)!}{r!} z_{m+r}^{(j)}(c\xi), \tag{25}$$

for the oblate ones, where $z_n^{(j)}(c\xi)$ is the nth order spherical Bessel, Neumann, and Hankel functions of the first and of the second kind in order of $j = 1, 2, 3$, and 4, respectively.

The spherical Bessel functions are regular in every finite domain of the $c\xi$ plane, including $c\xi = 0$, whereas the spherical Neumann functions have singularities at the origin $c\xi = 0$, where they become infinite. We shall, therefore, use the radial functions $R_{mn}^{(1)}$ but not $R_{mn}^{(2)}$ for representing the wave inside the spheroid and the incident wave. At very large distances from the spheroid, on the other hand, the scattered wave approaches a spherical diverging wave with center of the spheroid as its center. Thus, from the asymptotic behavior Eq. (22), the third kind function $R_{mn}^{(3)}$ is suitable to represent the scattered wave.

It is important to note that, as seen from Eqs. (13) and (19), the differential equations for the oblate spheroidal system can be obtained from those of the prolate system by the transformation

$$c \longrightarrow -ic, \qquad \xi \longrightarrow i\xi, \tag{26}$$

and vice versa. We shall use this transformation in the sequel to go from one system to the other.

The solutions of the scalar wave Eq. (12), which are used in the present study, are given by

$$\psi_{\substack{e\\o}\,mn}^{(j)}(c;\eta,\xi,\phi) = S_{mn}(c;\eta)R_{mn}^{(j)}(c;\xi)\begin{matrix}\cos\\\sin\end{matrix} m\phi, \tag{27}$$

for the prolate spheroidal system, and by

$$\psi_{\substack{e\\o}mn}^{(j)}(-ic;\eta, i\xi, \phi) = S_{mn}(-ic;\eta)R_{mn}^{(j)}(-ic;i\xi)\begin{matrix}\cos\\\sin\end{matrix} m\phi, \quad (28)$$

for the oblate one, respectively. In these equations the superscript j takes the values 1 or 3 depending on the usage of the radial functions of the first or third kind, and the suffixes e and o refer to even and odd dependence on ϕ (i.e., $\cos m\phi$ and $\sin m\phi$), respectively.

From these solutions of the scalar wave equation the following solutions of the vector wave equation can be formed[7]:

$$\mathbf{M}_{mn} = \nabla \times (\mathbf{a} \cdot \psi_{mn}), \quad (29)$$

and

$$\mathbf{N}_{mn} = k^{-1} \cdot \nabla \times \mathbf{M}_{mn}, \quad (30)$$

where the vector $\mathbf{a}$ is an arbitrary constant unit vector ($\mathbf{a} = \mathbf{e}$) or the position vector ($\mathbf{a} = \mathbf{r}$). The vectors $\mathbf{M}_{mn}$ and $\mathbf{N}_{mn}$ are solenoidal; then, the field vectors $\mathbf{E}$ and $\mathbf{H}$ can be expressed in infinite series of them. The vector function $\mathbf{M}_{mn}$ and $\mathbf{N}_{mn}$ are also related by

$$\mathbf{M}_{mn} = k^{-1} \cdot \nabla \times \mathbf{N}_{mn}. \quad (31)$$

In this study, we adopt the vector spheroidal wavefunctions

$$\mathbf{M}_{\substack{e\\o}mn}^{\ r} \text{ and } \mathbf{N}_{\substack{e\\o}mn}^{\ r},$$

which are formed from Eqs. (29) and (30) by using the scalar function Eq. (27) or Eq. (28), depending upon whether the spheroid is prolate or oblate, and by setting $\mathbf{a} = \mathbf{r}$, where $\mathbf{r}$ is the position vector. The explicit expression for the components of the spheroidal vector wavefunctions are listed in Flammer's book (Ref. 9, p. 74–77).

From Eqs. (11) and (22), it can be shown that the asymptotic forms of $\mathbf{M}_{mn}^{r(3)}$ and $\mathbf{N}_{mn}^{r(3)}$ in both cases of the prolate and oblate system, as $c\xi \to \infty$, become, by neglecting the terms of order higher than $1/r$, as follows:

$$M_{\substack{e\\o}mn,\eta}^{r(3)} \longrightarrow (-i)^{n+1} \cdot m\frac{S_{mn}(\cos\theta)}{\sin\theta}\frac{1}{kr}e^{ikr}\begin{matrix}\sin\\(-1)\cos\end{matrix} m\phi, \quad (32a)$$

$$M_{\substack{e\\o}mn,\phi}^{r(3)} \longrightarrow -(-i)^{n+1}\frac{dS_{mn}(\cos\theta)}{d\theta}\frac{1}{kr}e^{ikr}\begin{matrix}\cos\\\sin\end{matrix} m\phi, \quad (32b)$$

$$N_{\substack{e\\o}mn,\eta}^{r(3)} \longrightarrow -(-i)^{n}\frac{dS_{mn}(\cos\theta)}{d\theta}\frac{1}{kr}e^{ikr}\begin{matrix}\cos\\\sin\end{matrix} m\phi, \quad (33a)$$

$$N_{\substack{e\\o}mn,\phi}^{r(3)} \longrightarrow -(-i)^{n} \cdot m\frac{S_{mn}(\cos\theta)}{\sin\theta}\frac{1}{kr}e^{ikr}\begin{matrix}\sin\\(-1)\cos\end{matrix} m\phi. \quad (33b)$$

The radial components of $\mathbf{M}_{mn}^{r(3)}$ and $\mathbf{N}_{mn}^{r(3)}$ for large values of $c\xi$ tend to zero, then the scattered wave represented by $\mathbf{M}_{mn}^{r(3)}$ and $\mathbf{N}_{mn}^{r(3)}$ becomes a purely transverse wave at a large distance from the spheroid, as it must be.

IV. Series Expansion of the Field Vectors

It is assumed that the incident plane wave of unit amplitude is linearly polarized and that its direction of propagation makes an angle ζ with the positive z axis (Fig. 1).

We shall define, for oblique incidence ($\zeta \neq 0$), the incident plane as the plane specified by the z axis and the direction of propagation of the incident wave. The x axis is taken in the incident plane, and then $\phi = 0$ in that plane. When $\zeta = 0$ (parallel incidence) particularly, the x axis is taken to the direction of the electric vector of the incident wave propagating along the axis of revolution.

For oblique incidence, the polarized incident wave is resolved into two components as shown in Fig. 1: the TE mode for which the electric vector of the incident wave vibrates perpendicularly to the incident plane (case 1), and the TM mode for which the magnetic vector vibrates perpendicularly to this plane (case 2). For $\zeta \neq 0$, therefore, we shall consider two cases separately. At the parallel incidence, however, case 1 and case 2 yield the identical results due to the symmetry with respect to the incident wave.

Flammer[9] has developed the expansion of the polarized plane wave, propagating in the x,z plane to the direction making an angle ζ with the z axis, in terms of the prolate spheroidal vector wavefunctions

$$\mathbf{M}_{\substack{e\\o}mn}^{\ r(1)}(c;\eta, \xi, \phi) \text{ and } \mathbf{N}_{\substack{e\\o}mn}^{\ r(1)}(c;\eta, \xi, \phi)$$

as follows

$$\mathbf{e}_y \exp[ik(x \cdot \sin\zeta + z \cdot \cos\zeta)]$$
$$= -\sum_{m,n} i^n[g_{mn}(\zeta)\mathbf{M}_{emn}^{r(1)}(c;\eta, \xi, \phi) + if_{mn}(\zeta)\mathbf{N}_{omn}^{r(1)}(c;\eta, \xi, \phi)], \quad (34)$$

where the expansion coefficients $f_{mn}(\zeta)$ and $g_{mn}(\zeta)$ are given by

$$f_{mn}(\zeta) = \frac{4m}{\Lambda_{mn}}\sum_{r=0,1}^{\infty\prime}\frac{d_r^{mn}}{(r+m)(r+m+1)}\frac{P_{m+r}^{m}(\cos\zeta)}{\sin\zeta}, \quad (35)$$

$$g_{mn}(\zeta) = \frac{2(2-\delta_{0,m})}{\Lambda_{mn}}\sum_{r=0,1}^{\infty\prime}\frac{d_r^{mn}}{(r+m)(r+m+1)}\frac{dP_{m+r}^{m}(\cos\zeta)}{d\zeta}, \quad (36)$$

and the symbol

$$\sum_{m,n}$$

means the double summation over m and n as

$$\sum_{m=0}^{\infty}\sum_{n=m}^{\infty}$$

When $\zeta = 0$, all the coefficients with $m \neq 1$ vanish; and it follows that

$$f_{1n}(0) = g_{1n}(0) = 2\Lambda_{1n}^{-1}\sum_{r=0,1}^{\infty\prime} d_r^{1n}, \quad (37)$$

so the summation over m reduces to the single term with $m = 1$ throughout the following equations. This wave can also be expanded in terms of the oblate spheroidal vector wavefunctions, and the same results are obtained by replacing the prolate spher-

oidal vector wavefunctions with the oblate ones or by the transformation Eq. (26).

The incident wave of unit amplitude polarized in the TE mode (case 1) is described by

$$^{(i)}\mathbf{E} = -\mathbf{e}_y \cdot \exp[ik^{(I)}(x\sin\zeta + z\cdot\cos\zeta)], \tag{38}$$

$$^{(i)}\mathbf{H} = (\cos\zeta\cdot\mathbf{e}_x - \sin\zeta\cdot\mathbf{e}_z)\mathfrak{K}^{(I)}\exp[ik^{(I)}(x\sin\zeta + z\cdot\cos\zeta)] = (ik_0)^{-1}\cdot\nabla\times{}^{(i)}\mathbf{E}, \tag{39}$$

where $\mathbf{e}_x, \mathbf{e}_y$, and $\mathbf{e}_z$ are unit vectors along the x,y, and z axes, respectively. With the help of Eqs. (34), (30) and (31), the above incident field vectors are written in the form

$$\left.\begin{aligned} ^{(i)}\mathbf{E} &= \sum_{m,n} i^n[g_{mn}(\zeta)\mathbf{M}_{emn}{}^{r(1)} + if_{mn}(\zeta)\mathbf{N}_{omn}{}^{r(1)}], \\ ^{(i)}\mathbf{H} &= \mathfrak{K}^{(I)}\sum_{m,n} i^n[f_{mn}(\zeta)\mathbf{M}_{omn}{}^{r(1)} - ig_{mn}(\zeta)\mathbf{N}_{emn}{}^{r(1)}]. \end{aligned}\right\} \tag{40}$$

Similarly, for the incident wave polarized in the TM mode (case 2), the expression for the field vectors becomes

$$\left.\begin{aligned} ^{(i)}\mathbf{E} &= \sum_{m,n} i^n[f_{mn}(\zeta)\mathbf{M}_{omn}{}^{r(1)} - ig_{mn}(\zeta)\mathbf{N}_{emn}{}^{r(1)}], \\ ^{(i)}\mathbf{H} &= -\mathfrak{K}^{(I)}\sum_{m,n} i^n[g_{mn}(\zeta)\mathbf{M}_{emn}{}^{r(1)} + if_{mn}(\zeta)\mathbf{N}_{omn}{}^{r(1)}]. \end{aligned}\right\} \tag{41}$$

In order to apply to the boundary conditions, it is necessary to generate both the *TE* and *TM* modes in the internal and scattered waves corresponding to each polarization mode of the incident wave. They are set up in the same form as that of the incident wave as follows:

Case 1 (TE mode):

$$\left.\begin{aligned} ^{(s)}\mathbf{E} &= \sum_{m,n} i^n(\beta_{1,mn}\mathbf{M}_{emn}{}^{r(3)} + i\alpha_{1,mn}\mathbf{N}_{omn}{}^{r(3)}) \\ ^{(s)}\mathbf{H} &= \mathfrak{K}^{(I)}\sum_{m,n} i^n(\alpha_{1,mn}\mathbf{M}_{omn}{}^{r(3)} - i\beta_{1,mn}\mathbf{N}_{emn}{}^{r(3)}) \end{aligned}\right\}, (\xi > \xi_0); \tag{42}$$

and

$$\left.\begin{aligned} ^{(t)}\mathbf{E} &= \sum_{m,n} i^n(\delta_{1,mn}\mathbf{M}_{emn}{}^{r(1)} + i\gamma_{1,mn}\mathbf{N}_{omn}{}^{r(1)}) \\ ^{(t)}\mathbf{H} &= \mathfrak{K}^{(II)}\sum_{m,n} i^n(\gamma_{1,mn}\mathbf{M}_{omn}{}^{r(1)} - i\delta_{1,mn}\mathbf{N}_{emn}{}^{r(1)}) \end{aligned}\right\}, (\xi < \xi_0); \tag{43}$$

Case 2 (TM mode):

$$\left.\begin{aligned} ^{(s)}\mathbf{E} &= \sum_{m,n} i^n(\alpha_{2,mn}\mathbf{M}_{omn}{}^{r(3)} - i\beta_{2,mn}\mathbf{N}_{emn}{}^{r(3)}) \\ ^{(s)}\mathbf{H} &= -\mathfrak{K}^{(I)}\sum_{m,n} i^n(\beta_{2,mn}\mathbf{M}_{emn}{}^{r(3)} + i\alpha_{2,mn}\mathbf{N}_{omn}{}^{r(3)}) \end{aligned}\right\}, \quad (\xi > \xi_0); \tag{44}$$

and

$$\left.\begin{aligned} ^{(t)}\mathbf{E} &= \sum_{m,n} i^n(\gamma_{2,mn}\mathbf{M}_{omn}{}^{r(1)} - i\delta_{2,mn}\mathbf{N}_{emn}{}^{r(1)} \\ ^{(t)}\mathbf{H} &= -\mathfrak{K}^{(II)}\sum_{m,n} i^n(\delta_{2,mn}\mathbf{M}_{emn}{}^{r(1)} + i\gamma_{2,mn}\mathbf{N}_{omn}{}^{r(1)}) \end{aligned}\right\}, \quad (\xi < \xi_0); \tag{45}$$

where α_{mn}, β_{mn}, γ_{mn}, and δ_{mn} are the unknown coefficients with suffix 1 or 2 referring, respectively, to case 1 or case 2, and must be determined to satisfy the boundary conditions.

V. Formulation of the Boundary Conditions

The boundary conditions mentioned in Sec. II are written in the equivalent form as

$$\left.\begin{aligned} ^{(i)}E_\eta + {}^{(s)}E_\eta &= {}^{(t)}E_\eta, \quad ^{(i)}E_\phi + {}^{(s)}E_\phi = {}^{(t)}E_\phi \\ ^{(i)}H_\eta + {}^{(s)}H_\eta &= {}^{(t)}H_\eta, \quad ^{(i)}H_\phi + {}^{(s)}H_\phi = {}^{(t)}H_\phi \end{aligned}\right\} \text{at } \xi = \xi_0. \tag{46}$$

By virtue of the field expansions [Eqs. (40)–(45)], these conditions can be expressed explicitly in terms of the spheroidal wavefunctions. The resultant equations must hold for all allowed values of the coordinates $-1 \le \eta \le 1$ and $0 \le \phi \le 2\pi$, and may be used to determine the unknown coefficient α_{mn}, β_{mn}, γ_{mn}, and δ_{mn}. Because of the orthogonality of the trigonometric functions $\cos m\phi$ and $\sin m\phi$, in each expansion, the coefficients of the same ϕ-dependent trigonometric function must be equal, component by component; the equalities must hold for each corresponding term in the summation over m. For the summation over n, however, the individual terms in the series cannot be matched term by term. This is the cause of difficulty in determining the unknown coefficients.

The method used is as follows: the equations that stand for the continuity of η components are multiplied by $(\xi_0^2 \mp \eta^2)^{5/2} = [(\xi_0^2 \mp 1) \pm (1 - \eta^2)]^{5/2}$, and the equations for ϕ-components by $(\xi_0^2 \mp 1)^{-1/2}(\xi_0^2 \mp \eta^2)$, where these multipliers are positive in the full range of η; then all factors that are functions of η are replaced by the series of the associated Legendre functions of the first kind, which are orthogonal functions in the interval $-1 \le \eta \le 1$. For $m \ge 1$, the nine functions of η appear, and they can be expanded in terms of $P_{m-1+t}{}^{m-1}(\eta)$ as follows:

$$\text{(a)} \quad (1-\eta^2)^{1/2}S_{mn}(\eta) = \sum_{t=0}^{\infty} A_t{}^{mn}\cdot P_{m-1+t}{}^{m-1}(\eta), \tag{47}$$

$$\text{(b)} \quad (1-\eta^2)^{-1/2}S_{mn}(\eta) = \sum_{t=0}^{\infty} B_t{}^{mn}\cdot P_{m-1+t}{}^{m-1}(\eta), \tag{48}$$

$$\text{(c)} \quad \eta(1-\eta^2)^{1/2}S_{mn}(\eta) = \sum_{t=0}^{\infty} C_t{}^{mn}\cdot P_{m-1+t}{}^{m-1}(\eta), \tag{49}$$

$$\text{(d)} \quad \eta(1-\eta^2)^{-1/2}S_{mn}(\eta) = \sum_{t=0}^{\infty} D_t{}^{mn}\cdot P_{m-1+t}{}^{m-1}(\eta), \tag{50}$$

$$\text{(e)} \quad (1-\eta^2)^{3/2}S_{mn}(\eta) = \sum_{t=0}^{\infty} E_t{}^{mn}\cdot P_{m-1+t}{}^{m-1}(\eta), \tag{51}$$

$$\text{(f)} \quad \eta(1-\eta^2)^{3/2}S_{mn}(\eta) = \sum_{t=0}^{\infty} F_t{}^{mn}\cdot P_{m-1+t}{}^{m-1}(\eta), \tag{52}$$

$$\text{(g)} \quad (1-\eta^2)^{1/2}\frac{dS_{mn}(\eta)}{d\eta} = \sum_{t=0}^{\infty} G_t{}^{mn}\cdot P_{m-1+t}{}^{m-1}(\eta), \tag{53}$$

$$\text{(h)} \quad \eta(1-\eta^2)^{1/2}\frac{dS_{mn}(\eta)}{d\eta} = \sum_{t=0}^{\infty} H_t{}^{mn}\cdot P_{m-1+t}{}^{m-1}(\eta), \tag{54}$$

$$\text{(i)} \quad (1-\eta^2)^{3/2}\frac{dS_{mn}(\eta)}{d\eta} = \sum_{t=0}^{\infty} I_t{}^{mn}\cdot P_{m-1+t}{}^{m-1}(\eta). \tag{55}$$

For $m = 0$, however, only four functions are needed and can be expanded by the functions $P_{1+t}{}^{1}(\eta)$ as

$$(c') \quad \eta(1-\eta^2)^{1/2}S_{0n}(\eta) = \sum_{t=0}^{\infty} C_t^{0n} \cdot P_{1+t}^{1}(\eta), \tag{56}$$

$$(f') \quad \eta(1-\eta^2)^{3/2}S_{0n}(\eta) = \sum_{t=0}^{\infty} F_t^{0n} \cdot P_{1+t}^{1}(\eta), \tag{57}$$

$$(g') \quad (1-\eta^2)^{1/2}\frac{dS_{0n}(\eta)}{d\eta} = \sum_{t=0}^{\infty} G_t^{0n} \cdot P_{1+t}^{1}(\eta), \tag{58}$$

$$(i') \quad (1-\eta^2)^{3/2}\frac{dS_{0n}(\eta)}{d\eta} = \sum_{t=0}^{\infty} I_t^{0n} \cdot P_{1+t}^{1}(\eta). \tag{59}$$

The coefficients of these expansions are functions of c defined by Eq. (14) and can be evaluated by using Eq. (15) or (16), depending upon whether the spheroidal system is prolate or oblate, to express the angle function $S_{mn}(\eta)$ and its derivatives in terms of $P_{m+r}^{m}(\eta)$ and its derivatives. The evaluation of the integrals is somewhat troublesome, but the work is straightforward. Only the results are included, and these are listed below.

For $m \geq 1$,

$$A_t^{mn} = N_{m-1,m-1+t}^{-1} \cdot \sum_{r=0,1}{}' d_r^{mn} \times \int_{-1}^{+1} (1-\eta^2)^{1/2} P_{m+r}^{m}(\eta) P_{m-1+t}^{m-1}(\eta)\, d\eta, \tag{60}$$

$$= \begin{cases} 0, & (n-m)+t = \text{odd}, \\ \dfrac{(t+2m-1)(t+2m)}{(2t+2m+1)} d_t^{mn} \\ \quad - \dfrac{t(t-1)}{(2t+2m+3)} d_{t-2}^{mn}, & (n-m)+t = \text{even}, \end{cases}$$

$$B_t^{mn} = N_{m-1,m-1+t}^{-1} \cdot \sum_{r=0,1}{}' d_r^{mn} \times \int_{-1}^{+1} (1-\eta^2)^{-1/2} P_{m+r}^{m}(\eta) P_{m-1+t}^{m-1}(\eta)\, d\eta, \tag{61}$$

$$= \begin{cases} 0, & (n-m)+t = \text{odd}, \\ (2t+2m-1) \sum_{r=t}{}' d_r^{mn}, & (n-m)+t = \text{even}, \end{cases}$$

$$C_t^{mn} = N_{m-1,m-1+t}^{-1} \sum_{r=0,1}{}' d_r^{mn} \int_{-1}^{+1} \eta(1-\eta^2)^{1/2} P_{m+r}^{m}(\eta) P_{m-1+t}^{m-1}(\eta)\, d\eta, \tag{62}$$

$$= \begin{cases} 0, & (n-m)+t = \text{even}, \\ \dfrac{(t+2m-1)(t+2m)}{(2t+2m+1)} \left[\dfrac{(t+2m+1)}{(2t+2m+3)} d_{t+1}^{mn} + \dfrac{t}{(2t+2m-1)} d_{t-1}^{mn} \right] \\ \quad - \dfrac{t(t-1)}{(2t+2m-3)} \left[\dfrac{(t+2m-1)}{(2t+2m-1)} d_{t-1}^{mn} + \dfrac{(t-2)}{(2t+2m-5)} d_{t-3}^{mn} \right], & (n-m)+t = \text{odd}, \end{cases}$$

$$D_t^{mn} = N_{m-1,m-1+t}^{-1} \sum_{r=0,1}{}' d_r^{mn} \times \int_{-1}^{+1} \eta(1-\eta^2)^{-1/2} P_{m+r}^{m}(\eta) P_{m-1+t}^{m-1}(\eta)\, d\eta, \tag{63}$$

$$= \begin{cases} 0, & (n-m)+t = \text{even}, \\ t d_{t-1}^{mn} + (2t+2m-1) \sum_{r=t+1}{}' d_r^{mn}, & (n-m)+t = \text{odd}, \end{cases}$$

$$E_t^{mn} = N_{m-1,m-1+t}^{-1} \sum_{r=0,1}{}' d_r^{mn} \times \int_{-1}^{+1} (1-\eta^2)^{3/2} P_{m+r}^{m}(\eta) P_{m-1+t}^{m-1}(\eta)\, d\eta, \tag{64}$$

$$= \begin{cases} 0, & (n-m)+t = \text{odd}, \\ \dfrac{(t+2m-1)(t+2m)(t+2m+2)(t+2m+1)}{(2t+2m+1)(2t+2m+3)} \times \left[\dfrac{d_t^{mn}}{(2t+2m+1)} - \dfrac{d_{t+2}^{mn}}{(2t+2m+5)} \right] \\ \quad - \dfrac{2t(t-1)(t+2m)(t+2m-1)}{(2t+2m-3)(2t+2m+1)} \times \left[\dfrac{d_{t-2}^{mn}}{(2t+2m-3)} - \dfrac{d_t^{mn}}{(2t+2m+1)} \right] \\ \quad + \dfrac{t(t-1)(t-2)(t-3)}{(2t+2m-3)(2t+2m-5)} \times \left[\dfrac{d_{t-4}^{mn}}{(2t+2m-7)} - \dfrac{d_{t-2}^{mn}}{(2t+2m-3)} \right], & (n-m)+t = \text{even}, \end{cases}$$

$$F_t^{mn} = N_{m-1,m-1+t}^{-1} \sum_{r=0,1}{}' d_r^{mn} \times \int_{-1}^{+1} \eta(1-\eta^2)^{3/2} P_{m+r}^{m}(\eta)\, P_{m-1+t}^{m-1}(\eta)\, d\eta, \tag{65}$$

$$= \begin{cases} 0, & (n-m)+t = \text{even}, \\ \dfrac{(t+2m-1)(t+2m)(t+2m+1) \times (t+2m+2)(t+2m+3)}{(2t+2m+1)(2t+2m+3)(2t+2m+5)} \times \left[\dfrac{d_{t+1}^{mn}}{(2t+2m+3)} - \dfrac{d_{t+3}^{mn}}{(2t+2m+7)} \right] \\ \quad - \dfrac{t(t-2m)(t+2m+1)(t+2m)(t+2m-1)}{(2t+2m-3)(2t+2m+1)(2t+2m+3)} \times \left[\dfrac{d_{t-1}^{mn}}{(2t+2m-1)} - \dfrac{d_{t+1}^{mn}}{(2t+2m+3)} \right] \\ \quad - \dfrac{t(t-1)(t-2)(t+2m-1)(t+4m-1)}{(2t+2m-5)(2t+2m-3)(2t+2m+1)} \times \left[\dfrac{d_{t-3}^{mn}}{(2t+2m-5)} - \dfrac{d_{t-1}^{mn}}{(2t+2m-1)} \right] \\ \quad + \dfrac{t(t-1)(t-2)(t-3)(t-4)}{(2t+2m-3)(2t+2m-5)(2t+2m-7)} \times \left[\dfrac{d_{t-5}^{mn}}{(2t+2m-9)} - \dfrac{d_{t-3}^{mn}}{(2t+2m-5)} \right], & (n-m)+t = \text{odd}, \end{cases}$$

$$G_t^{mn} = N_{m-1,m-1+t}^{-1} \sum_{r=0,1}{}' d_r^{mn} \times \int_{-1}^{+1} (1-\eta^2)^{1/2} \frac{dP_{m+r}^{m}(\eta)}{d\eta} P_{m-1+t}^{m-1}(\eta)\,d\eta, \quad (66)$$

$$= \begin{cases} 0, & (n-m)+t = \text{even}, \\ -t(t+m-1)d_{t-1}^{mn} + m(2t+2m-1) \sum_{r=t+1}{}' d_r^{mn}, & (n-m)+t = \text{odd}, \end{cases}$$

$$H_t^{mn} = N_{m-1,m-1+t}^{-1} \sum_{r=0,1}{}' d_r^{mn} \int_{-1}^{+1} \eta(1-\eta^2)^{1/2} \frac{dP_{m+r}^{m}(\eta)}{d\eta} P_{m-1+t}^{m-1}(\eta)\,d\eta, \quad (67)$$

$$= \begin{cases} 0, & (n-m)+t = \text{odd}, \\ -\frac{t(t-1)(t+2m-2)}{(2t+2m-3)} d_{t-2}^{mn} - \frac{t(t-1)(2t+2m+1)+(t+2m)(t+2m-1)}{2(2t+2m+1)} d_t^{mn} + m(2t+2m-1) \sum_{r=t+2}{}' d_r^{mn}, & (n-m)+t = \text{even}, \end{cases}$$

$$I_t^{mn} = N_{m-1,m-1+t}^{-1} \sum_{r=0,1}{}' d_r^{mn} \int_{-1}^{+1} (1-\eta^2)^{3/2} \frac{dP_{m+r}^{m}(\eta)}{d\eta} P_{m-1+t}^{m-1}(\eta)\,d\eta, \quad (68)$$

$$= \begin{cases} 0, & (n-m)+t = \text{even}, \\ \frac{(t+2m)(t+2m-1)}{(2t+2m+1)} \left[\frac{(t+m+2)(t+2m+1)}{(2t+2m+3)} d_{t+1}^{mn} - \frac{t(m+t-1)}{(2t+2m-1)} d_{t-1}^{mn} \right] - \frac{t(t-1)}{(2t+2m-3} \left[\frac{(t+m)(t+2m-1)}{(2t+2m-1)} d_{t-1}^{mn} - \frac{(t-2)(t+m-3)}{(2t+2m-5)} d_{t-3}^{mn} \right], & (n-m)+t = \text{odd}, \end{cases}$$

where $N_{m-1,m-1+t}$ is the normalization constant for the function $P_{m-1+t}^{m-1}(\eta)$ and given by

$$N_{m-1,m-1+t} = \int_{-1}^{+1} [P_{m-1+t}^{m-1}(\eta)]^2 d\eta, = \frac{2\cdot(t+2m-2)!}{(2t+2m-1)\cdot t!}. \quad (69)$$

For $m = 0$,

$$C_t^{0n} = N_{1,1+t}^{-1} \sum_{r=0,1}{}' d_r^{0n} \int_{-1}^{+1} \eta(1-\eta^2)^{1/2} P_r^0(\eta) P_{1+t}^1(\eta)\,d\eta, \quad (70)$$

$$= \begin{cases} 0, & n+t = \text{even}, \\ \frac{1}{(2t+1)} \left[\frac{(t+1)}{(2t+3)} d_{t+1}^{0n} + \frac{t}{(2t-1)} d_{t-1}^{0n} \right] - \frac{1}{(2t+5)} \left[\frac{(t+3)}{(2t+7)} d_{t+3}^{0n} + \frac{(t+2)}{(2t+3)} d_{t+1}^{0n} \right], & n+t = \text{odd}, \end{cases}$$

$$F_t^{0n} = N_{1,1+t}^{-1} \sum_{r=0,1}{}' d_r^{0n} \int_{-1}^{+1} \eta(1-\eta^2)^{3/2} P_r^0(\eta) P_{1+t}^1(\eta)\,d\eta, \quad (71)$$

$$= \begin{cases} 0, & n+t = \text{even}, \\ \frac{(t+3)(t+4)(t+5)}{(2t+5)(2t+7)} \left[\frac{d_{t+1}^{0n}}{(2t+3)(2t+5)} - \frac{2d_{t+3}^{0n}}{(2t+5)(2t+9)} + \frac{d_{t+5}^{0n}}{(2t+9)(2t+11)} \right] + \frac{3t(t+3)}{(2t+1)(2t+5)} \left[\frac{d_{t-1}^{0n}}{(2t-1)(2t+1)} - \frac{2d_{t+1}^{0n}}{(2t+1)(2t+5)} + \frac{d_{t+3}^{0n}}{(2t+5)(2t+7)} \right] - \frac{t(t-1)(t-2)}{(2t-1)(2t+1)} \left[\frac{d_{t-3}^{0n}}{(2t-5)(2t-3)} - \frac{2d_{t-1}^{0n}}{(2t-3)(2t+1)} + \frac{d_{t+1}^{0n}}{(2t+1)(2t+3)} \right], & n+t = \text{odd}, \end{cases}$$

$$G_t^{0n} = N_{1,1+t}^{-1} \sum_{r=0,1}{}' d_r^{0n} \int_{-1}^{+1} (1-\eta^2)^{1/2} \frac{dP_r^0(\eta)}{d\eta} P_{1+t}^1(\eta)\,d\eta, \quad (72)$$

$$= \begin{cases} 0, & n+t = \text{even}, \\ d_{t+1}^{0n}, & n+t = \text{odd}, \end{cases}$$

$$I_t^{0n} = N_{1,1+t}^{-1} \sum_{r=0,1}{}' d_r^{0n} \int_{-1}^{+1} (1-\eta^2)^{3/2} \frac{dP_r^0(\eta)}{d\eta} P_{1+t}^1(\eta)\,d\eta, \quad (73)$$

$$= \begin{cases} 0, & n+t = \text{even}, \\ \frac{1}{2t+1} \left[\frac{(t+1)(t+2)}{(2t+3)} d_{t+1}^{0n} - \frac{t(t-1)}{(2t-1)} d_{t-1}^{0n} \right] - \frac{1}{2t+5} \left[\frac{(t+3)(t+4)}{(2t+7)} d_{t+3}^{0n} - \frac{(t+1)(t+2)}{(2t+3)} d_{t+1}^{0n} \right], & (n+t) = \text{odd}, \end{cases}$$

where

$$N_{1,1+t} = \int_{-1}^{+1} [P_{1+t}^1(\eta)]^2 d\eta, = \frac{2(t+1)(t+2)}{(2t+3)}, \quad (74)$$

Inserting Eqs. (47)–(55) for $m \geq 1$, or Eqs. (56)–(59) for $m = 0$, into the equations representing the boundary conditions, and then considering the orthogonality of the associated Legendre functions of the first kind, it can be seen that the individual terms in the summation over t must be matched term by term.

For easier manipulation of the equations, we shall here employ the following substitutions, for $m \geq 1$, defined by

$$U_{mn}^{(j),t}(c^{(h)}) = m\xi_0 R_{mn}^{(j)}(c^{(h)};\xi_0)[(\xi_0^2-1)^2 B_t^{mn}(c^{(h)}) + 2(\xi_0^2-1)A_t^{mn}(c^{(h)}) + E_t^{mn}(c^{(h)})], \quad (75)$$

$$V_{mn}^{(j),t}(c^{(h)}) = \frac{i}{c^{(h)}}\left\{\frac{m^2}{(\xi_0^2-1)}R_{mn}^{(j)}(c^{(h)};\xi_0)[(\xi_0^2-1)^2 D_t^{mn}(c^{(h)}) + 2(\xi_0^2-1)C_t^{mn}(c^{(h)}) + F_t^{mn}(c^{(h)})] - R_{mn}^{(j)}(c^{(h)};\xi_0)\left[\lambda_{mn}(c^{(h)}) - (c^{(h)}\xi_0)^2 + \frac{m^2}{\xi_0^2-1}\right] \times [(\xi_0^2-1)C_t^{mn}(c^{(h)}) + F_t^{mn}(c^{(h)})] + \xi_0(\xi_0^2-1) \times \left[\frac{dR_{mn}^{(j)}(c^{(h)};\xi)}{d\xi}\right]_{\xi_0}[2C_t^{mn}(c^{(h)}) + (\xi_0^2-1)G_t^{mn}(c^{(h)}) + I_t^{mn}(c^{(h)})] + R_{mn}^{(j)}(c^{(h)};\xi_0)[(\xi_0^2-1)^2 G_t^{mn}(c^{(h)}) + (3\xi_0^2-1)I_t^{mn}(c^{(h)})]\right\}, \quad (76)$$

$$X_{mn}^{(j),t}(c^{(h)}) = \xi_0 R_{mn}^{(j)}(c^{(h)};\xi_0)G_t^{mn}(c^{(h)}) - \left[\frac{dR_{mn}^{(j)}(c^{(h)};\xi)}{d\xi}\right]_{\xi_0} \cdot C_t^{mn}(c^{(h)}), \quad (77)$$

$$Y_{mn}^{(j),t}(c^{(h)}) = \frac{i}{c^{(h)}}\, m\,((\xi_0^2-1)^{-1}R_{mn}^{(j)}(c^{(h)};\xi_0)\,[A_t^{mn}(c^{(h)}) + H_t^{mn}(c^{(h)})] + \{R_{mn}^{(j)}(c^{(h)};\xi_0) + \xi_0[dR_{mn}^{(j)}(c^{(h)};\xi)/d\xi]_{\xi_0}\}B_t^{mn}(c^{(h)})), \quad (78)$$

in the prolate spheroidal system and

$$U_{mn}^{(j),t}(-ic^{(h)}) = m\xi_0 R_{mn}^{(j)}(-ic^{(h)};i\xi_0)[(\xi_0^2+1)^2 \times B_t^{mn}(-ic^{(h)}) - 2(\xi_0^2+1)A_t^{mn}(-ic^{(h)}) + E_t^{mn}(-ic^{(h)})], \quad (79)$$

$$V_{mn}^{(j),t}(-ic^{(h)}) = \frac{i}{c^{(h)}}\left\{-\frac{m^2}{(\xi_0^2+1)}R_{mn}^{(j)}(-ic^{(h)};i\xi_0) \times [(\xi_0^2+1)^2 D_t^{mn}(-ic^{(h)}) - 2(\xi_0^2+1)C_t^{mn}(-ic^{(h)}) + F_t^{mn}(-ic^{(h)})] + R_{mn}^{(j)}(-ic^{(h)};i\xi_0)\left[\lambda_{mn}(-ic^{(h)}) - (c^{(h)}\xi_0)^2 - \frac{m^2}{\xi_0^2+1}\right][(\xi_0^2+1)C_t^{mn}(-ic^{(h)}) - F_t^{mn}(-ic^{(h)})] + \xi_0(\xi_0^2+1)\left[\frac{dR_{mn}^{(j)}(-ic^{(h)},i\xi)}{d\xi}\right]_{\xi_0} \times [-2C_t^{mn}(-ic^{(h)}) + (\xi_0^2+1)G_t^{mn}(-ic^{(h)}) - I_t^{mn}(-ic^{(h)})] + R_{mn}^{(j)}(-ic^{(h)};i\xi_0)[(\xi_0^2+1)^2 \times G_t^{mn}(-ic^{(h)}) - (3\xi_0^2+1)I_t^{mn}(-ic^{(h)})]\right\}, \quad (80)$$

$$X_{mn}^{(j),t}(-ic^{(h)}) = \xi_0 R_{mn}^{(j)}(-ic^{(h)};i\xi_0)G_t^{mn}(-ic^{(h)}) + \left[\frac{dR_{mn}^{(j)}(-ic^{(h)};i\xi)}{d\xi}\right]_{\xi_0} C_t^{mn}(-ic^{(h)}), \quad (81)$$

$$Y_{mn}^{(j),t}(-ic^{(h)}) = \frac{i}{c^{(h)}}\, m\Big(-(\xi_0^2+1)^{-1}R_{mn}^{(j)}(-ic^{(h)};i\xi_0)[A_t^{mn}(-ic^{(h)}) + H_t^{mn}(-ic^{(h)})] + \Big\{R_{mn}^{(j)} \times (-ic^{(h)};i\xi_0) + \xi_0\left[\frac{dR_{mn}^{(j)}(-ic^{(h)};i\xi)}{d\xi}\right]_{\xi_0}\Big\} \times B_t^{mn}(-ic^{(h)})\Big), \quad (82)$$

in the oblate one, respectively. In these expressions the superscript j takes, as already mentioned, the value 1 or 3, according to the radial functions of the first or third kind, and the superscript h on c is I or II referring to the outer or inner region of the spheroid, respectively. For $m = 0$, these parameters are found to become

$$U_{0n}^{(j),t} = Y_{0n}^{(j),t} = 0, \quad (83)$$

$$V_{0n}^{(j),t} = \frac{i}{c^{(h)}}\left\{\mp R_{0n}^{(j)}[\lambda_{0n} - (c^{(h)}\xi_0)^2][(\xi_0^2 \mp 1)C_t^{0n} \pm F_t^{0n}] + \xi_0(\xi_0^2 \mp 1)\left(\frac{dR_{0n}^{(j)}}{d\xi}\right)_{\xi_0}[\pm 2C_t^{0n} + (\xi_0^2 \mp 1)G_t^{0n} \pm I_t^{0n}] + R_{0n}^{(j)}[(\xi_0^2 \mp 1)^2 G_t^{0n} \pm (3\xi_0^2 \mp 1)I_t^{0n}]\right\}, \quad (84)$$

$$X_{0n}^{(j),t} = \xi_0 R_{0n}^{(j)} \cdot G_t^{0n} \mp \left[\frac{dR_{0n}^{(j)}}{d\xi}\right]_{\xi_0} C_t^{0n}. \quad (85)$$

The parameters $U_{mn}^{(j),t}$ and $V_{mn}^{(j),t}$ correspond to the η components of the vector functions $\mathbf{M}_{mn}^{r(j)}$ and $\mathbf{N}_{mn}^{r(j)}$, and also $X_{mn}^{(j),t}$ and $Y_{mn}^{(j),t}$ are related to the ϕ components of them, respectively. With these parameters, the equations for determining the unknown coefficients in the prolate spheroidal system, for instance, are now written, for each value of m, in the form:

Case 1 (TE mode):

$$E_\eta: \sum_{n=m}^{\infty} i^n[V_{mn}^{(3),t}(c^{(I)})\cdot\alpha_{1,mn} + U_{mn}^{(3),t}(c^{(I)})\cdot\beta_{1,mn} - V_{mn}^{(1),t}(c^{(II)})\cdot\gamma_{1,mn} - U_{mn}^{(1),t}(c^{(II)})\cdot\delta_{1,mn}] = -\sum_{n=m}^{\infty} i^n[f_{mn}(\zeta)\cdot V_{mn}^{(1),t}(c^{(I)}) + g_{mn}(\zeta)\cdot U_{mn}^{(1),t}(c^{(I)})], \quad (86a)$$

$$E_\phi: \sum_{n=m}^{\infty} i^n[Y_{mn}^{(3),t}(c^{(I)})\cdot\alpha_{1,mn} + X_{mn}^{(3),t}(c^{(I)})\cdot\beta_{1,mn} - Y_{mn}^{(1),t}(c^{(II)})\cdot\gamma_{1,mn} - X_{mn}^{(1),t}(c^{(II)})\cdot\delta_{1,mn}] = -\sum_{n=m}^{\infty} i^n[f_{mn}(\zeta)\cdot Y_{mn}^{(1),t}(c^{(I)}) + g_{mn}(\zeta)\cdot X_{mn}^{(1),t}(c^{(I)})], \quad (86b)$$

$$H_\eta: \sum_{n=\infty}^{\infty} i^n[U_{mn}^{(3),t}(c^{(I)})\cdot\alpha_{1,mn} + V_{mn}^{(3),t}(c^{(I)})\cdot\beta_{1,mn} - \mathcal{H}U_{mn}^{(1)t}(c^{(II)})\cdot\gamma_{1,mn} - \mathcal{H}V_{mn}^{(1)t}(c^{(II)})\cdot\delta_{1,mn}] = -\sum_{n=m}^{\infty} i^n[f_{mn}(\zeta)\cdot U_{mn}^{(1),t}(c^{(I)}) + g_{mn}(\zeta)\cdot V_{mn}^{(1),t}(c^{(I)})], \quad (86c)$$

$$H_\phi: \sum_{n=m}^{\infty} i^n[X_{mn}^{(3),t}(c^{(I)})\cdot\alpha_{1,mn} + Y_{mn}^{(3),t}(c^{(I)})\cdot\beta_{1,mn} - \mathcal{H}X_{mn}^{(1),t}(c^{(II)})\cdot\gamma_{mn} - \mathcal{H}Y_{mn}^{(1),t}(c^{(II)})\cdot\delta_{1,mn}] = -\sum_{n=m}^{\infty} i^n[f_{mn}(\zeta)\cdot X_{mn}^{(1),t}(c^{(I)}) + g_{mn}(\zeta)Y_{mn}^{(1),t}(c^{(I)})], \quad (m = 0,1,2,\ldots;\ t = 0,1,2,\ldots) \quad (86d)$$

Case 2 (TM mode):

$$E_\eta: \sum_{n=m}^{\infty} i^n[U_{mn}^{(3),t}(c^{(I)})\cdot\alpha_{2,mn} + V_{mn}^{(3),t}(c^{(I)})\cdot\beta_{2,mn} - U_{mn}^{(1),t}(c^{(II)})\gamma_{2,mn} - V_{mn}^{(1),t}(c^{(II)})\delta_{2,mn}] = -\sum_{n=m}^{\infty} i^n[f_{mn}(\zeta)U_{mn}^{(1),t}(c^{(I)}) + g_{mn}(\zeta)V_{mn}^{(1),t}(c^{(I)})], \quad (87a)$$

$$E_\phi: \sum_{n=m}^{\infty} i^n[X_{mn}^{(3),t}(c^{(I)})\cdot\alpha_{2,mn} + Y_{mn}^{(3),t}(c^{(I)})\cdot\beta_{2,mn} - X_{mn}^{(1),t}(c^{(II)})\cdot\gamma_{2,mn} - Y_{mn}^{(1),t}(c^{(II)})\cdot\delta_{2,mn}] = -\sum_{n=m}^{\infty} i^n[f_{mn}(\zeta)\cdot X_{mn}^{(1),t}(c^{(I)}) + g_{mn}(\zeta)Y_{mn}^{(1),t}(c^{(I)})], \quad (87b)$$

$$H_\eta: \sum_{n=m}^{\infty} i^n[V_{mn}^{(3),t}(c^{(I)})\cdot\alpha_{2,mn} + U_{mn}^{(3),t}(c^{(I)})\cdot\beta_{2,mn} - \mathcal{H}V_{mn}^{(1),t}(c^{(II)})\cdot\gamma_{2,mn} - \mathcal{H}U_{mn}^{(1),t}(c^{(II)})\cdot\delta_{2,mn}] = -\sum_{n=m}^{\infty} i^n[f_{mn}(\zeta)V_{mn}^{(1),t}(c^{(I)}) + g_{mn}(\zeta)\cdot U_{mn}^{(1),t}(c^{(I)})], \quad (87c)$$

$$H_\phi: \sum_{n=m}^{\infty} i^n[Y_{mn}^{(3),t}(c^{(I)})\cdot\alpha_{2,mn} + X_{mn}^{(3),t}(c^{(I)})\beta_{2,mn} - \mathcal{H}Y_{mn}^{(1),t}(c^{(II)})\gamma_{2,mn} - \mathcal{H}X_{mn}^{(1),t}(c^{(II)})\cdot\delta_{2,mn}] = -\sum_{n=m}^{\infty} i^n[f_{mn}(\zeta)Y_{mn}^{(1),t}(c^{(I)}) + g_{mn}(\zeta)\cdot X_{mn}^{(1),t}(c^{(I)})], \quad (87d)$$

$$(m = 0,1,2,\ldots;\ t = 0,1,2,\ldots)$$

where

$$\mathcal{H} = \mathcal{H}^{(II)}/\mathcal{H}^{(I)}. \quad (88)$$

The parameter $\mathcal{H}$ is the (complex) refractive index of the spheroid relative to the surrounding medium. The equations in the oblate spheroidal system can be obtained for each case of the polarization by replacing the parameters $U_{mn}^{(j),t}$, $V_{mn}^{(j),t}$, $X_{mn}^{(j),t}$, and $Y_{mn}^{(j),t}$ for the prolate spheroidal system with those for the oblate one.

Thus, the equations used to determine the unknown coefficients constitute an infinite system of coupled linear equations with complex coefficients. These equations are valid for each value of t, so that by taking t sufficiently large an adequate number of relations between unknown coefficients is generated. The convergence of the infinite series is expected both physically and mathematically, as shown by Siegel *et al.*[6] and by Wait.[10] Practically, the infinite system of equations is truncated to a finite number of equations in the same number of unknown, and the standard numerical techniques are employed to solve them. It is also worth noting that, because of the relations

$$U_{mn}^{(j),t} = Y_{mn}^{(j),t} = 0, \text{ for } (n-m)+t = \text{odd}, \quad (89)$$

and

$$V_{mn}^{(j),t} = X_{mn}^{(j),t} = 0, \text{ for } (n-m)+t = \text{even}, \quad (90)$$

which are deduced from the behavior of the expansion coefficients Eqs. (60)–(68) or Eqs. (70)–(73) and the definition of these parameters, the term involving even-ordered functions ($n - m + t$ = even) are completely decoupled from those of odd-order ($n - m + t$ = odd), and this saves a great deal of labor needed to solve the system as discussed in detail later.

Thus, in principle, the problem of scattering of the electromagnetic wave by a homogeneous spheroid has been solved. The fields not only scattered but also within the spheroid can be obtained at once.

VI. Scattered Fields at Infinity

Equations (42) and (44) for case 1 and case 2, respectively, with the appropriate values of the expansion coefficients determined by the method stated in the previous section, are the expressions for the field vectors of the scattered wave, which are valid for all values of the coordinates (η,ξ,ϕ).

Usually one is more interested in the behavior of the scattered wave at relatively large distances from the scatterer. The scattered field at infinity can be deduced by taking the asymptotic form of ${}^{(s)}\mathbf{E}$ and ${}^{(s)}\mathbf{H}$, as $c^{(I)}\xi \to \infty$, under the assumption that $c^{(I)} = 2\pi l/\lambda^{(I)}$ does not equal zero; hereafter $c^{(I)}$ will be called the size parameter of the spheroid, in analogy to that of Mie scattering.

By virtue of the asymptotic behaviors Eqs. (32a)–(33b) for the vector functions $\mathbf{M}_{mn}^{r(3)}$ and $\mathbf{N}_{mn}^{r(3)}$, one obtains such asymptotic forms of the scattered fields in each spheroidal system as:

Case 1 (TE mode):

$$-{}^{(s)}E_{1,\eta} = {}^{(s)}H_{1,\phi}/\mathcal{H}^{(I)} = \frac{i\lambda^{(I)}}{2\pi r}\exp i2\pi r/\lambda^{(I)} \times \sum_{m,n}\left[\alpha_{1,mn}\frac{dS_{mn}(\cos\theta)}{d\theta} + \beta_{1,mn}\cdot m\frac{S_{mn}(\cos\theta)}{\sin\theta}\right]\sin m\phi, \quad (91a)$$

$${}^{(s)}E_{1,\phi} = {}^{(s)}H_{1,\eta}/\mathcal{H}^{(I)} = \frac{i\lambda^{(I)}}{2\pi r}\exp i2\pi r/\lambda^{(I)} \times \sum_{m,n}\left[\alpha_{1,mn}\cdot m\frac{S_{mn}(\cos\theta)}{\sin\theta} + \beta_{1,mn}\frac{dS_{mn}(\cos\theta)}{d\theta}\right]\cos m\phi, \quad (91b)$$

Case 2 (TM mode):

$${}^{(s)}E_{2,\eta} = -{}^{(s)}H_{2,\phi}/\mathcal{H}^{(I)} = \frac{i\lambda^{(I)}}{2\pi r}\exp i2\pi r/\lambda^{(I)} \times \sum_{m,n}\left[\alpha_{2,mn}\cdot m\frac{S_{mn}(\cos\theta)}{\sin\theta} + \beta_{2,mn}\frac{dS_{mn}(\cos\theta)}{d\theta}\right]\cos m\phi, \quad (92a)$$

$${}^{(s)}E_{2,\phi} = {}^{(s)}H_{2,\eta}/\mathcal{H}^{(I)} = \frac{i\lambda^{(I)}}{2\pi r}\exp i2\pi r/\lambda^{(I)} \times \sum_{m,n}\left[\alpha_{2,mn}\frac{dS_{mn}(\cos\theta)}{d\theta} + \beta_{2,mn}m\frac{S_{mn}(\cos\theta)}{\sin\theta}\right]\sin m\phi, \quad (92b)$$

where the radial components ${}^{(s)}E_\xi$, ${}^{(s)}H_\xi$ fall off as $(\lambda^{(I)}/r)^2$, so that they may be neglected in the far-field zone. The components ${}^{(s)}E_\eta$ and ${}^{(s)}E_\phi$ are perpendicular to each other, and the phase relation between them is arbitrary; the scattered wave will, in general, be elliptically polarized.

For the sake of convenience, we shall here introduce the amplitude functions and the intensity functions for oblique and parallel incidences separately.

(i) Oblique Incidence ($\zeta \neq 0$)

At oblique incidence, the amplitude functions for the incident wave of the TE and TM modes (or case 1 and case 2), respectively, are written in the form:

Case 1:

$$T_{11}(\theta,\phi) = \sum_{m,n} [\alpha_{1,mn} \cdot \sigma_{mn}(\theta) + \beta_{1,mn} \cdot \chi_{mn}(\theta)] \cos m\phi, \quad (93)$$

$$T_{12}(\theta,\phi) = \sum_{m,n} [\alpha_{1,mn} \cdot \chi_{mn}(\theta) + \beta_{1,mn} \cdot \sigma_{mn}(\theta)] \sin m\phi, \quad (94)$$

Case 2:

$$T_{21}(\theta,\phi) = \sum_{m,n} [\alpha_{2,mn} \cdot \chi_{mn}(\theta) + \beta_{2,mn} \cdot \sigma_{mn}(\theta)] \sin m\phi, \quad (95)$$

$$T_{22}(\theta,\phi) = \sum_{m,n} [\alpha_{2,mn} \cdot \sigma(\theta) + \beta_{2,mn} \cdot \chi_{mn}(\theta)] \cos m\phi, \quad (96)$$

where $\sigma_{mn}(\theta)$ and $\chi_{mn}(\theta)$ are the angular functions that are depending on the size parameter $c^{(I)}$ and are defined by

$$\sigma_{mn}(\theta) = m[S_{mn}(\cos\theta)/\sin\theta], \quad (97)$$

$$\chi_{mn}(\theta) = (d/d\theta)[S_{mn}(\cos\theta)], \quad (98)$$

and these functions, when $\theta = 0, \pi$, become zero except the ones with $m = 1$.

Thus,

$$\sigma_{mn}(0) = \chi_{mn}(0) = \begin{cases} 0, & (m \neq 1), \\ \frac{1}{2} \sum_{r=0,1}{}' (r+1)(r+2) d_r^{1n}, & (m = 1). \end{cases} \quad (99)$$

The amplitude functions T_{11}, T_{22}, T_{12}, T_{21} correspond, respectively, to the elements A_1, A_2, A_3, and A_4 of the amplitude matrix discussed by van de Hulst (Ref. 11, p. 43).

The intensities of scattered light, at infinity, polarized in the η (or $-\theta$) and ϕ azimuths are given by:

Case 1:

$$I_{1,\phi} = {}^{(s)}E_{1,\phi} \cdot {}^{(s)}E_{1,\phi}{}^{*} = (\lambda^{2(I)}/4\pi^2 r^2) i_{11}(\theta,\phi), \quad (100a)$$

$$I_{1,\eta} = {}^{(s)}E_{1,\eta} \cdot {}^{(s)}E_{1,\eta}{}^{*} = (\lambda^{2(I)}/4\pi^2 r^2) i_{12}(\theta,\phi). \quad (100b)$$

Case 2:

$$I_{2,\phi} = {}^{(s)}E_{2,\phi} \cdot {}^{(s)}E_{2,\phi}{}^{*} = (\lambda^{2(I)}/4\pi^2 r^2) i_{21}(\theta,\phi), \quad (101a)$$

$$I_{2,\eta} = {}^{(s)}E_{2,\eta} \cdot {}^{(s)}E_{2,\eta}{}^{*} = (\lambda^{2(I)}/4\pi^2 r^2) i_{22}(\theta,\phi), \quad (101b)$$

where ${}^{(s)}E_{\phi}{}^{*}$ and ${}^{(s)}E_{\eta}{}^{*}$ are the complex conjugates of ${}^{(s)}E_{\phi}$ and ${}^{(s)}E_{\eta}$, respectively, and i_{11}, i_{12}, i_{21}, and i_{22} will be called the intensity functions at oblique incidence and are written, in terms of the amplitude functions, as

$$i_{11}(\theta,\phi) = |T_{11}(\theta,\phi)|^2, \quad (102)$$

$$i_{12}(\theta,\phi) = |T_{12}(\theta,\phi)|^2, \quad (103)$$

$$i_{21}(\theta,\phi) = |T_{21}(\theta,\phi)|^2, \quad (104)$$

$$i_{22}(\theta,\phi) = |T_{22}(\theta,\phi)|^2. \quad (105)$$

The intensity functions i_{11} give the intensity components of the scattered light, which is perpendicular (TE mode) to the scattering plane specified by the direction of the scattered wave and by the z axis, where the incident light of unit intensity is also perpendicular (TE mode) to the incident plane containing the direction of the incident wave and the z axis. The intensity functions i_{12} give the parallel components (TM mode) for the same incident wave. When the incident wave is of the TM mode, the intensity components of the scattered light perpendicular and parallel to the scattering plane are given by the intensity functions i_{21} and i_{22}, respectively. Thus, the intensity functions i_{11} and i_{22} are the components polarized in the same mode to the incident wave, while i_{12} and i_{21} are the cross-polarized components.

(ii) Parallel Incidence ($\zeta = 0$):

In this case, the scattered intensities are

$$I_{\phi} = (\lambda^{2(I)}/4\pi^2 r^2) \cdot i_1(\theta) \cdot \sin^2\phi, \quad (106a)$$

$$I_{n} = (\lambda^{2(I)}/4\pi^2 r^2) \cdot i_1(\theta) \cdot \cos^2\phi, \quad (106b)$$

where $i_1(\theta)$ and $i_2(\theta)$ will be called the intensity functions at the parallel incidence, corresponding, respectively, to the components perpendicular and parallel to the scattering plane and are given by

$$i_1(\theta) = \left| \sum_{n=1}^{\infty} [\alpha_{1n} \cdot \chi_{1n}(\theta) + \beta_{1n} \cdot \sigma_{1n}(\theta)] \right|^2, \quad (107)$$

$$i_2(\theta) = \left| \sum_{n=1}^{\infty} [\alpha_{1n} \cdot \sigma_{1n}(\theta) + \beta_{1n} \cdot \chi_{1n}(\theta)] \right|^2, \quad (108)$$

which are in a form similar to the intensity functions for the scattering by a homogeneous sphere (Mie scattering). The angular functions $\sigma_{1n}(\theta)$ and $\chi_{1n}(\theta)$ have the same behavior, respectively, as the angular functions $\pi_n(\cos\theta)$ and $\tau_n(\cos\theta)$ introduced by van de Hulst (Ref. 11, p. 125). The scattering plane is here defined as the plane specified by the directions of the incident wave (or the z axis) and the scattered wave. Then the angle θ just measures the scattering angle.

VII. Extinction and Scattering Cross Sections

A. Extinction Cross Section

With incident wave polarized linearly, the extinction cross section C_{ext} is proportional to a certain amplitude component of the scattered wave; the amplitude is that which corresponds to forward scattering, and the component is in the direction of the electric vector of the incident wave.[8,11]

The amplitude component of the scattered wave in the direction of the electric vector of the incident wave ($\phi = 0$), for forward scattering ($\theta = \zeta$), is given, for case 1, by

$$-{}^{(s)}E_{1,\phi}\big|_{\theta=\zeta,\phi=0} = -\frac{i\lambda^{(I)}}{2\pi r} \exp i2\pi r/\lambda^{(I)} \cdot T_{11}(\zeta,0),$$

$$= -\frac{i \cdot \lambda^{(I)}}{2\pi r} \exp i2\pi r/\lambda^{(I)} \cdot \sum_{m,n} [\alpha_{1,mn}\sigma_{mn}(\zeta) + \beta_{1,mn}\chi_{mn}(\zeta)]; \quad (109)$$

then, the extinction cross section is written as follows:

$$C_{1,ext} = -\frac{\lambda^{2(I)}}{\pi} \mathrm{Re} \sum_{m,n} [\alpha_{1,mn} \cdot \sigma_{mn}(\zeta) + \beta_{1,mn} \cdot \chi_{mn}(\zeta)], \quad (110)$$

where Re denotes the real part.

For case 2 (TM mode), one can obtain in a similar way

$$C_{2,\mathrm{ext}} = -\frac{\lambda^{2(\mathrm{I})}}{\pi}\,\mathrm{Re}\sum_{m,n}[\alpha_{2,mn}\cdot\sigma_{mn}(\zeta) + \beta_{2,mn}\cdot\chi_{mn}(\zeta)]. \tag{111}$$

The extinction cross section C_{ext} is naturally the functions of the size parameter $c^{(\mathrm{I})}$, the relative refractive index of the spheroid $\mathfrak{K}$, and the incident angle ζ.

At parallel incidence ($\zeta = 0$), using Eq. (99), the extinction cross section becomes

$$C_{\mathrm{ext}} = -\frac{\lambda^{2(\mathrm{I})}}{\pi}\cdot\sum_{n=1}^{\infty}\Big[{\sum_{r=0,1}}'\frac{(r+1)(r+2)}{2}d_r^{1n}\Big] \times \mathrm{Re}\,(\alpha_{1n} + \beta_{1n}). \tag{112}$$

(B.) Scattering Cross Section

The scattering cross section C_{sca} is defined as the ratio between the rate of dissipation of the scattered energy and the rate at which the energy is incident on unit cross-sectional area of the scattering obstacle and is given, for example, for case 1 at oblique incidence by

$$C_{1,\mathrm{sca}} = \frac{1}{k^{(\mathrm{I})2}}\int[i_{11}(\theta,\phi) + i_{12}(\theta,\phi)]d\Omega,$$
$$= \frac{1}{k^{(\mathrm{I})2}}\int_0^{2\pi}\int_0^{\pi}[\,|T_{11}(\theta,\phi)|^2 + |T_{12}(\theta,\phi)|^2]\sin\theta d\theta d\phi. \tag{113}$$

Inserting Eqs. (93) and (94) into this equation and by using formulas

$$\int_0^{2\pi}\sin m\phi\cdot\sin m'\phi d\phi = \int_0^{2\pi}\cos m\phi\cdot\cos m'\phi d\phi = \begin{cases}0, & (m \neq m')\\ \pi, & (m = m')\end{cases} \tag{114}$$

and

$$\int_0^{\pi}[\sigma_{mn}(\theta)\cdot\chi_{mn}(\theta) + \sigma_{mn}(\theta)\cdot\chi_{mn}(\theta)]\sin\theta d\theta = 0, \tag{115}$$

the integral Eq. (113) can be evaluated, leading to

$$C_{1,\mathrm{sca}} = \frac{\lambda^{2(\mathrm{I})}}{4\pi}\sum_{m=0}\sum_{n=m}\sum_{n'=m} \times \Pi_{nn'}^{\ m}\mathrm{Re}(\alpha_{1,mn}\cdot\alpha_{1,mn'}^{*} + \beta_{1,mn}\cdot\beta_{1,mn'}^{*}), \tag{116}$$

where the asterisk denotes the complex conjugate and the coefficient $\Pi_{nn'}^{\ m}$ is given by

$$\Pi_{nn'}^{\ m} = \int_0^{\pi}[\sigma_{mn}(\theta)\cdot\sigma_{mn'}(\theta) + \chi_{mn}(\theta)\cdot\chi_{mn'}(\theta)]\sin\theta d\theta,$$
$$= \begin{cases}0, & |n-n'| = \text{odd},\\ {\sum_{r=0,1}}'\dfrac{2(r+m)(r+m+1)(r+2m)!}{(2r+2m+1)r!}d_r^{\ mn}d_r^{\ mn'}, & |n-n'| = \text{even}.\end{cases} \tag{117}$$

Similarly, the scattering cross section for case 2 at oblique incidence is written as

$$C_{2,\mathrm{sca}} = \frac{\lambda^{2(\mathrm{I})}}{4\pi}\sum_{m=0}\sum_{n=m}\sum_{n'=m} \Pi_{nn'}^{\ m}\,\mathrm{Re}(\alpha_{2,mn}\cdot\alpha_{2,mn'}^{*} + \beta_{2,mn}\cdot\beta_{2,mn'}^{*}). \tag{118}$$

When $\zeta = 0$, the scattering cross section becomes

$$C_{\mathrm{sca}} = \frac{\lambda^{2(\mathrm{I})}}{4\pi}\sum_{n=1}\sum_{n'=1}\Pi_{nn'}^{\ 1}\cdot\mathrm{Re}(\alpha_{1n}\cdot\alpha_{1n'}^{*} + \beta_{1n}\cdot\beta_{1n'}^{*}), \tag{119}$$

where the coefficient $\Pi_{nn'}^{\ 1}$ *is given by*

$$\Pi_{nn'}^{\ 1} = \begin{cases}0, & |n-n'| = \text{odd},\\ {\sum_{r=0,1}}'\dfrac{2(r+1)^2(r+2)^2}{(2r+3)}d_r^{\ 1n}d_r^{\ 1n'}, & |n-n'| = \text{even}.\end{cases} \tag{120}$$

VIII. Discussions

(1) In the study on the dielectric coated prolate spheroidal antenna, Yeh[12] proposed a useful method of handling the boundary-value problem, and his method was used by Wait[10] for the prolate spheroidal antenna with a confocal sheath. The basic idea of their method is to represent the spheroidal angle functions in the dielectric regions as expansions of the natural angle functions of the outer region. This suggests, to our study, another representation for the functions of η, instead of the series expansions by the associated Legendre functions of the first kind in Sec. V, in terms of such angle functions in the ambient medium, of order $m - 1$ for $m \geq 1$, as $S_{m-1,m-1+t}(c^{(\mathrm{I})};\eta)$ and of order 1 for $m = 0$, as $S_{1,1+t}(c^{(\mathrm{I})};\eta)$.

For example, we write

$$(1-\eta^2)^{1/2}S_{mn}(c^{(h)};\eta) = \sum_{t=0}^{\infty}\bar{A}_t^{\ mn}(c^{(h)})\cdot S_{m-1,m-1+t}(c^{(\mathrm{I})};\eta), \tag{121}$$

where $\bar{A}_t^{\ mn}$ is the expansion coefficient with an appended bar to distinguish from $A_t^{\ mn}$ in Sec. V, and is given by

$$\bar{A}_t^{\ mn}(c^{(h)}) = \Lambda_{m-1,m-1+t}^{\ -1}(c^{(\mathrm{I})})\cdot \int_{-1}^{+1}(1-\eta^2)^{1/2}\cdot S_{mn}(c^{(\mathrm{I})};\eta)\cdot S_{m-1,m-1+t}(c^{(\mathrm{I})};\eta)d\eta, \tag{122}$$

$$= \begin{cases}0, & (n-m)+t = \text{odd},\\ \Lambda_{m-1,m-1+t}^{\ -1}(c^{(\mathrm{I})}){\sum_{\lambda=0,1}}'\dfrac{d_\lambda^{\ m-1,m-1+t}(c^{(\mathrm{I})})}{(2\lambda+2m-1)} \Big[\dfrac{2(\lambda+2m)!}{(2\lambda+2m+1)\lambda!}d_\lambda^{\ mn}(c^{(h)}) - \dfrac{2(\lambda+2m-2)!}{(2\lambda+2m-3)(\lambda-2)!}d_{\lambda-2}^{\ mn}(c^{(h)})\Big], & (n-m)+t = \text{even},\end{cases}$$

where $\Lambda_{m-1,m-1+t}(c^{(\mathrm{I})})$ is the normalization constant

given by Eq. (18) for the angle function $S_{m-1,m-1+t}(c^{(I)};\eta)$. The coefficient $\bar{A}_t^{mn}$ is also related to A_t^{mn} by

$$\bar{A}_t^{mn}(c^{(h)}) = \Lambda_{m-1,m-1+t}^{-1}(c^{(I)})\cdot \sum_{\lambda=0,1}{}' d_\lambda^{m-1,m-1+t}(c^{(I)}) \cdot N_{m-1,m-1+\lambda}\cdot A_t^{mn}(c^{(h)}), \quad (123)$$

where $N_{m-1,m-1+t}$ is the normalization constant given by Eq. (69) for the associated Legendre functions of the first kind. In a similar way, we can obtain other expansion coefficients in the same form as Eq. (123) by using the coefficients for the expansions in terms of the associated Legendre functions. The method used by Schultz[5] is, in essence, identical with this approach.

The relative advantage of this approach over that used in Sec. V remains to be investigated. As pointed out by Wait,[10] it seems that when the properties of the inner and outer regions are nearly the same, the expansions of the angle functions in one region in terms of those in another region may be highly convergent, and that, for electrically large spheroids, the expansion in terms of Legendre functions may be very poorly convergent. We have calculated both series, Eq. (47) and Eq. (121), and showed that at least for the values of $c \lesssim 10$ the rapidity of convergence of the two series is almost the same and moreover the values of expansion coefficients A_t^{mn} and $\bar{A}_t^{mn}$ are nearly equal. This is evident from the fact that the representation of the spheroidal angle functions given by Eqs. (15) and (16) is dominated by the term where $r = n - m$ for those small values of c. Therefore, so long as c is not too large, the expansions in terms of the associated Legendre functions are preferable to those in terms of the spheroidal angle functions, because of the simpler form to calculate.

(2) When the spheroid is a perfect conductor or $\mathcal{K} \to \infty$, the electromagnetic field cannot be sustained within the spheroid and the boundary condition for a perfect conductor that the tangential components of the electric vectors must vanish at the surface

$$\left.\begin{aligned} {}^{(i)}E_\eta + {}^{(s)}E_\eta &= 0,\\ {}^{(i)}E_\phi + {}^{(s)}E_\phi &= 0,\end{aligned}\right\} \quad \text{at } \xi = \xi_0. \quad (124)$$

is only demanded. Then the system of equations determining the unknown expansion coefficients α_{mn} and β_{mn} becomes, for each m, as follows:

$$\sum_{n=m}^{\infty} i^n[V_{mn}^{(3),t}(c^{(I)})\cdot\alpha_{1,mn} + U_{mn}^{(3),t}(c^{(I)})\cdot\beta_{1,mn}] = -\sum_{n=m}^{\infty} i^n[f_{mn}(\zeta)\cdot V_{mn}^{(1),t}(c^{(I)}) + g_{mn}(\zeta)\cdot U_{mn}^{(1),t}(c^{(I)})], \quad (125a)$$

$$\sum_{n=m}^{\infty} i^n[Y_{mn}^{(3),t}(c^{(I)})\cdot\alpha_{1,mn} + X_{mn}^{(3),t}(c^{(I)})\cdot\beta_{1,mn}] = -\sum_{n=m}^{\infty} i^n[f_{mn}(\zeta)\cdot Y_{mm}^{(1),t}(c^{(I)}) + g_{mn}(\zeta)\cdot X_{mn}^{(1),t}(c^{(I)})], \quad (125b)$$

$$(m = 0,1,2,\ldots; l = 0,1,2,\ldots)$$

for case 1, and

$$\sum_{n=m}^{\infty} i^n[U_{mn}^{(3),t}(c^{(I)})\cdot\alpha_{2,mn} + V_{mn}^{(3),t}(c^{(I)})\cdot\beta_{2,mn}] = -\sum_{n=m}^{\infty} i^n[f_{mn}(\zeta)\cdot U_{mn}^{(1),t}(c^{(I)}) + g_{mn}(\zeta)V_{mn}^{(1),t}(c^{(I)})], \quad (126a)$$

$$\sum_{n=m}^{\infty} i^n[X_{mn}^{(3),t}(c^{(I)})\cdot\alpha_{2,mn} + Y_{mn}^{(3),t}(c^{(I)})\cdot\beta_{2,mn}] = -\sum_{n=m}^{\infty} i^n[f_{mn}(\zeta)\cdot X_{mn}^{(1),t}(c^{(I)}) + g_{mn}(\zeta)\cdot Y_{mn}^{(1),t}(c^{(I)})], \quad (126b)$$

$$(m = 0,1,2,\ldots; t = 0,1,2,\ldots)$$

for case 2, respectively.

(3) By virtue of Eqs. (89) and (90), as previously stated, one can divide the system of equations determining the unknown coefficients into two subsystems: one that involves the even-ordered coefficients α_{mn} and γ_{mn} ($n - m$ = even) and odd-ordered β_{mn} and δ_{mn} ($n - m$ = odd), and one that involves α_{mn} and γ_{mn} of odd-order and β_{mn} and δ_{mn} of even-order.

When t = odd = $2s + 1$ ($s = 0,1,2,\ldots$), the system of Eqs. (86a) to (86d), for example, becomes

$$\sum_{n=m}{}'\{i^n[V_{mn}^{(3),2s+1}(c^{(I)})\cdot\alpha_{1,mn} - V_{mn}^{(1),2s+1}(c^{(II)})\cdot\gamma_{1,mn}] + i^{n+1}[U_{mn+1}^{(1),2s+1}(c^{(I)})\cdot\beta_{1,mn+1} - U_{mn+1}^{(1),2s+1}(c^{(II)})\cdot\delta_{1,mn+1}]\} = -\sum_{n=m}{}'[i^n f_{mn}(\zeta)V_{mn}^{(1),2s+1}(c^{(I)}) + i^{n+1}g_{mn+1}(\zeta)U_{mn+1}^{(1),2s+1}(c^{(I)}], \quad (127a)$$

$$\sum_{n=m}{}'\{i^n[X_{mn}^{(3),2s+1}(c^{(I)})\cdot\alpha_{1,mn} - \mathcal{K}X_{mn}^{(1),2s+1}(c^{(II)})\cdot\gamma_{1,mn}] + i^{n+1}[Y_{mn+1}^{(3),2s+1}(c^{(I)})\cdot\beta_{1,mn+1} - \mathcal{K}Y_{mn+1}^{(1),2s+1}(c^{(II)})\cdot\delta_{1,mn+1}]\} = -\sum_{n=m}{}'[i^n f_{mn}(\zeta)\cdot X_{mn}^{(1),2s+1}(c^{(I)}) + i^{n+1}g_{mn+1}(\zeta)\cdot Y_{mn+1}^{(1),2s+1}(c^{(I)})], \quad (127b)$$

$$\sum_{n=m}{}'\{i^{n+1}[U_{mn+1}^{(3),2s+1}(c^{(I)})\cdot\alpha_{1,mn+1} - \mathcal{K}U_{mn+1}^{(1),2s+1}(c^{(II)})\cdot\gamma_{1,mn+1}] + i^n[V_{mn}^{(3),2s+1}(c^{(I)})\cdot\beta_{1,mn} - \mathcal{K}V_{mn}^{(1),2s+1}(c^{(II)})\cdot\delta_{1,mn}]\} = -\sum_{n=m}{}'[i^{n+1}f_{mn+1}(\zeta)U_{mn+1}^{(1),2s+1}(c^{(I)}) + i^n g_{mn}(\zeta)V_{mn}^{(1),2s+1}(c^{(I)})], \quad (127c)$$

$$\sum_{n=m}{}'\{i^{n+1}[Y_{mn+1}^{(3),2s+1}(c^{(I)})\cdot\alpha_{1,mn+1} - Y_{mn+1}^{(1),2s+1}(c^{(II)})\cdot\gamma_{1,mn+1}] + i^n[X_{mn}^{(3),2s+1}(c^{(I)})\cdot\beta_{1,mn} - X_{mn}^{(1),2s+1}(c^{(II)})\cdot\delta_{1,mn}]\} = -\sum_{n=m}{}'[i^{n+1}f_{mn+1}(\zeta)\cdot Y_{mn+1}^{(1),2s+1}(c^{(I)}) + i^n g_{mn}(\zeta)X_{mn}^{(1),2s+1}(c^{(I)})], \quad (127d)$$

and when t = even = $2s$ (s = 0,1,2, . . .); on the other hand, it becomes as follows:

$$\sum_{n=m}{}' \{ i^{n+1} [V_{mn+1}{}^{(3),2s}(c^{(I)}) \cdot \alpha_{1,mn+1} - V_{mn+1}{}^{(1),2s}(c^{(II)}) \cdot \gamma_{1,mn+1}] + i^{n} [U_{mn}{}^{(3),2s}(c^{(I)}) \cdot \beta_{1,mn} - U_{mn}{}^{(1),2s}(c^{(II)}) \cdot \delta_{1,mn}] \} = - \sum_{n=m}{}' [i^{n+1} f_{mn+1}(\xi) V_{mn+1}{}^{(1),2s}(c^{(I)}) + i^{n} g_{mn}(\xi) U_{mn}{}^{(1),2s}(c^{(I)})], \quad (128a)$$

$$\sum_{n=m}{}' \{ i^{n+1} [X_{mn+1}{}^{(3),2s}(c^{(I)}) \cdot \alpha_{1,mn+1} - \mathcal{K} \cdot X_{mn+1}{}^{(1),2s}(c^{(II)}) \cdot \gamma_{1,mn+1}] + i^{n} [Y_{mn}{}^{(3),2s}(c^{(I)}) \cdot \beta_{1,mn} - \mathcal{K} Y_{mn}{}^{(1),2s}(c^{(II)}) \cdot \delta_{1,mn}] \} = - \sum_{n=m}{}' [i^{n+1} f_{mn+1}(\xi) \cdot X_{mn+1}{}^{(1),2s}(c^{(I)}) + i^{n} g_{mn}(\xi) \cdot Y_{mn}{}^{(1),2s}(c^{(I)})], \quad (128b)$$

$$\sum_{n=m}{}' \{ i^{n} [U_{mn}{}^{(3),2s}(c^{(I)}) \cdot \alpha_{1,mn} - \mathcal{K} U_{mn}{}^{(1),2s}(c^{(II)}) \cdot \gamma_{1,mn}] + i^{n+1} [V_{mn+1}{}^{(3),2s}(c^{(I)}) \cdot \beta_{1,mn+1} - \mathcal{K} V_{mn+1}{}^{(1),2s}(c^{(II)}) \cdot \delta_{1,mn+1}] \} = - \sum_{n=m}{}' [i^{n} f_{mn}(\xi) U_{mn}{}^{(1),2s}(c^{(I)}) + i^{n+1} g_{mn+1}(\xi) \cdot V_{mn+1}{}^{(1),2s}(c^{(I)})], \quad (128c)$$

$$\sum_{n=m}{}' \{ i^{n} [Y_{mn}{}^{(3),2s}(c^{(I)}) \cdot \alpha_{1,mn} - Y_{mn}{}^{(1),2s}(c^{(III)}) \cdot \gamma_{1,mn}] + i^{n+1} [X_{mn+1}{}^{(3),2s}(c^{(I)}) \cdot \beta_{1,mn+1} - X_{mn+1}{}^{(1),2s}(c^{(II)}) \cdot \delta_{1,mn+1}] \} = - \sum_{n=m}{}' [i^{n} f_{mn}(\xi) Y_{mn}{}^{(1),2s}(c^{(I)}) + i^{n+1} g_{mn+1}(\xi) \cdot X_{mn+1}{}^{(1),2s}(c^{(I)})], \quad (128d)$$

where $\Sigma_{n=m}{}'$ means the summation over values as $n = m, m + 2\ m + 4, \ldots$. In these equations, Eqs. (127a), (127b), (128c), and (128d) are combining the even-order terms of $\alpha_{1,mn}$ and $\gamma_{1,mn}$ with the odd-order terms of $\beta_{1,mn}$ and $\delta_{1,mn}$, whereas Eqs. (127c), (127d), (128a), and (128b) combine the odd-ordered $\alpha_{1,mn}$ and $\gamma_{1,mn}$ with even-ordered $\beta_{1,mn}$ and $\delta_{1,mn}$. Therefore, when the infinite system of Eqs. (86a) to (86d) is truncated to the finite number of equations including only the first N expansion coefficients for $\alpha_{1,mn}$, $\beta_{1,mn}$, $\gamma_{1,mn}$, and $\delta_{1,mn}$ ($n = m, m + 1, \ldots, m + N - 1$) for each value of m, we can use, to detrmine the coefficients, such two systems of $2N$-linear-coupled equations as (127a), (127b), (128c), and (128d) and as (127c), (127d), (128a), and (128b), instead of solving the system of $4N$-linear Eqs. (86a) to (86d). This implies marked simplification and improvement in calculating the unknown coefficients.

Now, it must be remembered that the parameters $U_{mn}{}^{(3),t}$, $V_{mn}{}^{(3),t}$, $X_{mn}{}^{(3),t}$ and $Y_{mn}{}^{(3),t}$ are complex and that the magnitudes of the real and imaginary parts of them are in great disparity, particularly for large values of n, because they involve both $R_{mn}{}^{(1)}$ and $R_{mn}{}^{(2)}$, where the absolute value of $R_{mn}{}^{(1)}$ decreases as n increases; on the other hand, $R_{mn}{}^{(2)}$ increases in magnitude. By definitions of the parameters, furthermore, the magnitudes of real and imaginary parts for $U_{mn}{}^{(j),t}$ and $V_{mn}{}^{(j),t}$ behave in a different manner, for example, when the real part of $U_{mn}{}^{(j),t}$ is large, the imaginary part of $V_{mn}{}^{(j),t}$ becomes large, and vice versa. A similar relation holds for $X_{mn}{}^{(j),t}$ and $Y_{mn}{}^{(j),t}$. These behaviors make practical computation of the unknown coefficients unstable. In order to avoid such difficulty, the system of equations for the combination of, for instance, even-ordered $\alpha_{1,mn}$ and odd-ordered $\beta_{1,mn}$ in case 1 can be derived by taking Eqs. (127a) + (127b), Eqs. (127a) − (127b), Eqs. (128c) + (128d), and Eqs. (128c) − (128d) and by dividing the coefficients of the system of equations by $R_{mn}{}^{(2)}(c^{(I)}; \xi_0)$ or by $R_{mn}{}^{(1)}(c^{(II)}; \xi_0)$, for the purpose of making the magnitudes of real and imaginary parts and the absolute values of all coefficients uniform.

IX. Numerical Computation

In our theory, solutions are expressed in terms of the spheroidal wavefunctions, which are functions not only of the coordinates but also of the properties of the medium. One disadvantage in using the spheroidal functions is that numerical tables of these functions are, at present, scanty and sporadic and in order to find numerical values, very laborious computations are necessary. Flammer[9] has published extensive tables of numerical values for the spheroidal eigenvalues, expansion coefficients, and functions themselves, which were compiled from earlier workers and, in part, evaluated by himself. However, his tables are not enough, particularly, for large values of c and for the oblate spheroidal functions. No table exists for complex values of c, which are needed for the case of an absorbing spheroid, in which the refractive index $\mathcal{K}$ is complex. We shall, in this study, adopt only the real index $\mathcal{K}$ = 1.33. The numerical values of the spheroidal eigenvalues and expansion coefficients were computed following the scheme developed by Bouwkamp,[13] which is also cited in Flammer's monograph.

Numerical computations are performed on the spheroids of the size parameters c = 1 up to 7, where the superscript (I) on c is omitted, and with the ratio of the semimajor axis a to the semiminor axis b of a/b = 2, 5, and 10 for the prolate spheroids, and a/b = 2 for the oblate ones. The eccentricity e of the ellipse can be expressed in terms of the ratio a/b and its numerical values for a/b = 2, 5, and 10 are, respectively, 0.866025, 0.979796, and 0.994987. The incident angles ζ are taken to be 0°, 45°, and 90°.

Several checks on the validity of the results obtained have been made for some quantities. As a check on the convergence of the infinite series for the fields expressions, which were practically truncated to finite series including only the first N expansion coefficients α_{1n} and β_{1n}, the scattering and extinction cross sections at parallel incidence were computed for various values of N. In Fig. 2, the cross sections, which are normalized by those with the largest N values, for the prolate spheroids of c = 1 and c = 5, and with a/b = 2 (left half) and a/b = 10 (right half) are shown by solid lines for the extinction and by dashed lines for the scattering. Since the refractive index is real, the extinction and scattering cross sections, which are, respectively, computed from Eqs.

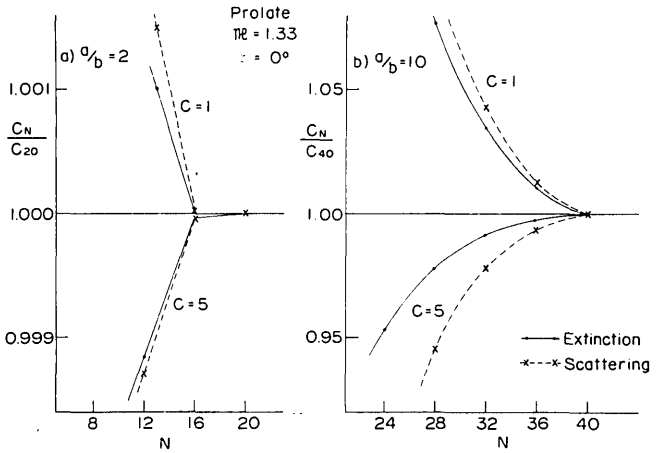

Fig. 2. The extinction and scattering cross sections at $\zeta = 0°$ computed by truncating infinite series to finite ones including only first N terms, as a function of the termination number for the truncation N. The cross sections, normalized by those with the largest N values, for the prolate spheroids of $c = 1$ and 5, and of $a/b = 2$ (left half) and $a/b = 10$ (right half) are shown by solid lines for extinction and by dashed lines for scattering.

(112) and (119), should coincide. It is seen from the figures that the series converge more rapidly for the spheroids of $a/b = 2$ than for those of $a/b = 10$, and the rapidity of convergence is not so much dependent on the size parameter c, and that, as N increases, the normalized cross sections for $c = 1$ converge decreasingly to the finite values, while for $c = 5$, they tend to converge increasingly. In fact, at least for $c \lesssim 10$, the scattering and extinction cross sections for the spheroid of $a/b = 2$ agree through five or more places for $N = 20$, and those for $a/b = 10$ coincide through three or more places for $N = 40$. At oblique incidence, the convergence of the summations over m (i.e., ϕ-dependent series) are dependent on the size and shape of the spheroid. It seems enough for the terminated number M of the terms of ϕ-dependent series to set up $M = 3$ for $c \lesssim 3$ and $M \approx c$ for $3 < c \lesssim 10$ ($m = 0,1,2, \ldots, M$).

X. Angular Distribution of the Scattered Intensity

A. Parallel Incidence of the Linearly Polarized Light

At parallel incidence ($\zeta = 0°$) of the linearly polarized light, the intensity functions i_1 and i_2, defined by Eqs. (107) and (108), are functions, for the spheroid of given size and shape, of the refractive index $\mathfrak{M}$ and of the scattering angle Θ and correspond, respectively, to the components perpendicular and parallel to the scattering plane.

The angular distribution of the intensity functions scattered by the prolate spheroids of $a/b = 2$ and $\mathfrak{M} = 1.33$ are shown in Fig. 3 for several size parameters from $c = 1$ to $c = 7$. The components i_1 are given by solid curves and the components i_2 by dashed ones. The ordinates in these figures are on a logarithmic scale, while the abscissa is linear in the scattering angle Θ measured from the forward direction. The values of the scattering functions for $\Theta = 0°$ and $\Theta = 180°$ are indicated in the margin. For a small spheroid of $c = 1$, the angular pattern of i_1 is rather flat; on the other hand, that of i_2 is approximately proportional to $\cos^2\Theta$. This is similar to the behavior of the Rayleigh limit for the scattering by very small spheres: for the limit of $c \ll 1$, the scattering by a spheroid becomes independent of its shape and the angular distribution coincides with that of the so-called Rayleigh scattering, in which i_1 is constant and i_2 varies as $\cos^2\Theta$. With the increase of size parameter c, the magnitude of the intensity functions increases and the values for $\Theta = 0°$ become much greater than for $\Theta = 180°$ (i.e., the predominance of the forward scattering); in addition, the patterns of their angular distributions become more and more complicated, showing oscillating fluctuations with Θ particularly, for the component i_1.

The corresponding picture for the prolate spheroids of $a/b = 5$ is given in Fig. 4. the basic behavior of the intensity functions with regard to the increase of c, is the same as that for $a/b = 2$. If Fig. 3 is compared with Fig. 4, some effects of the shape (or the

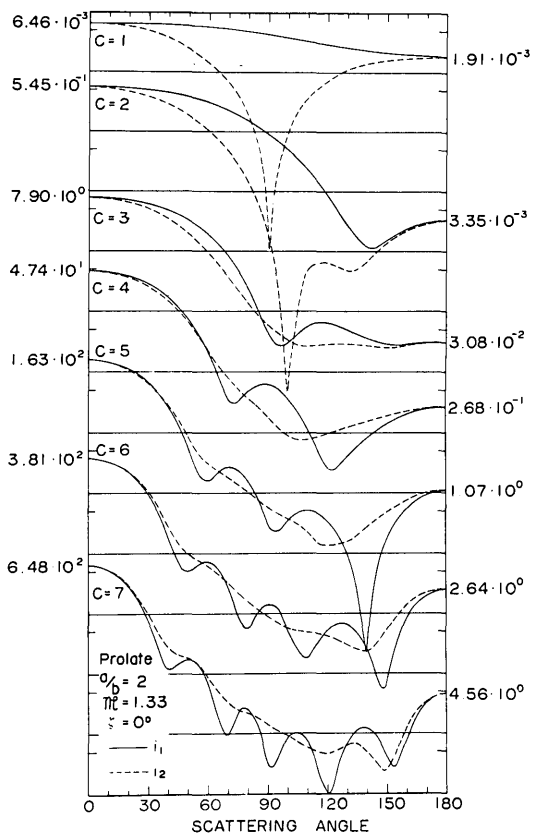

Fig. 3. Angular distribution of the intensity functions i_1 (solid lines) and i_2 (dashed lines) at $\zeta = 0°$ for the prolate spheroids of $a/b = 2$ and $c = 1$ up to 7. The ordinate is on a logarithmic scale (1 division = a factor 10), and the abscissa is linear in the scattering angle. The values for the forescattering and backscattering are indicated in the margin.

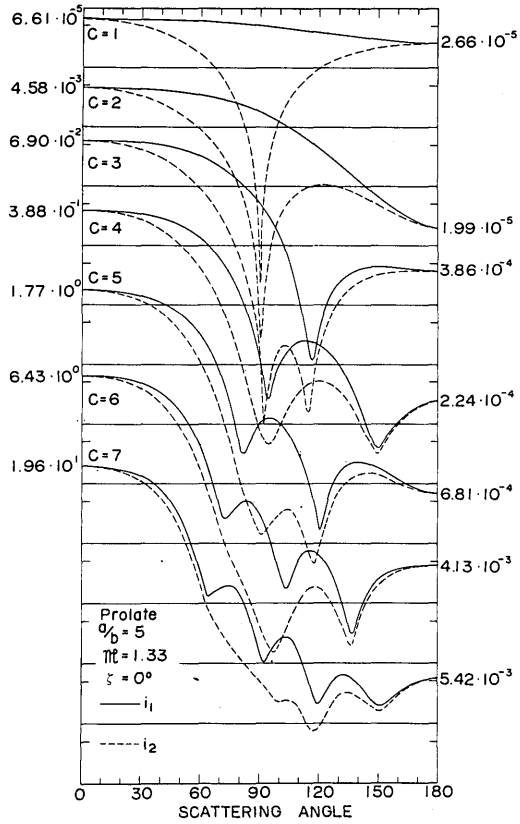

Fig. 4. Same as Fig. 3, but for the prolate spheroid of $a/b = 5$.

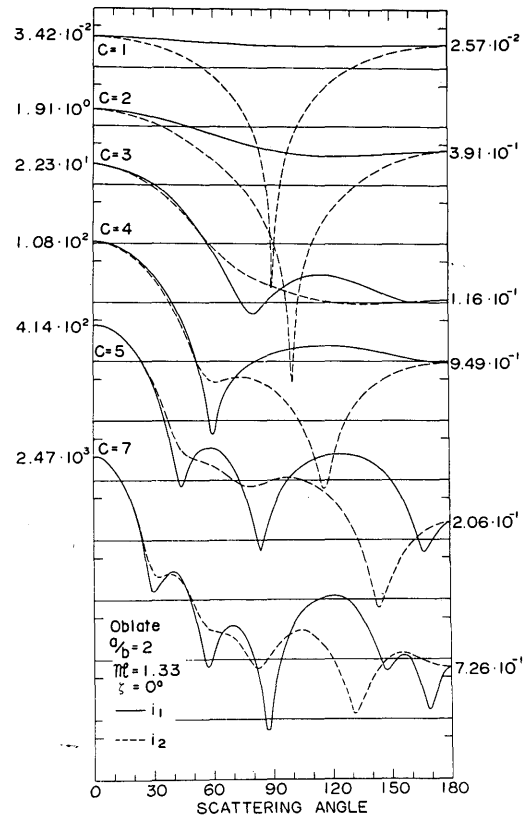

Fig. 5. Same as Fig. 3, but for the oblate spheroid of $a/b = 2$.

degree of prolateness) are clearly observed: as the spheroids become slender, the angular patterns for both i_1 and i_2 fluctuate more and more with the scattering angle. The patterns for the spheroids of $a/b = 2$ fairly resemble those for spheres (cf. Ref. 11, p. 153). For the spheroids of a given size parameter, the over-all magnitude of the intensity functions is diminished, and the difference of values for $\Theta = 0°$ and $\Theta = 180°$ is enlarged, as the ratio a/b increases.

As an example of scattering by oblate spheroids, the intensity functions for $a/b = 2$ are displayed in Fig. 5. This figure shows the effects of the shape on the angular distribution patterns. In comparison with Fig. 3, the larger magnitudes than those for the prolate spheroids and the broad maxima of i_1 at the scattering angles around 120° can be regarded as their characteristic features.

B. Oblique Incidence of the Linearly Polarized Light

The scattered intensity functions at the oblique incidence of the linearly polarized light are given by i_{11} and i_{12} for case 1 and by i_{21} and i_{22} for case 2, which are, respectively, defined by Eqs. (102), (103), (104), and (105). The numerical results for these functions are given as functions of angles θ and ϕ, where θ and ϕ are, respectively, the zenith and azimuth angles in the spherical coordinates with its origin at the center of the spheroid. The x axis is taken in the incident plane, then $\phi = 0$ in this plane. The scattering angle Θ between the directions of the incident wave $(\zeta,0)$ and of the scattered one (θ,ϕ) can easily be obtained from the spherical geometry as follows:

$$\cos\Theta = \cos\zeta\cdot\cos\theta + \sin\zeta\cdot\sin\theta\cdot\cos\phi. \quad (129)$$

Figure 6 shows the angular distribution of the intensity functions i_{11} (solid lines) and i_{12} (dashed lines) scattered by the prolate spheroid of $c = 1$ and $a/b = 2$ for the incident light polarized in the TE mode (case 1) at $\zeta = 45°$. The magnitude of the scattered intensity can be evaluated from the linear scale plotted in the negative z axis. This figure illustrates, as a function of θ in the circular diagram, the angular patterns in three scattering planes through the z axis: one parallel to the incident plane (i.e., $\phi = 0°$ or 180°), one inclining from it by an angle 45° (i.e., $\phi =$ 45° or 225°), and one normal to it (i.e., $\phi = 90°$ or 270°), which we shall call, for sake of convenience, plane 1, plane 2 and plane 3, respectively. The perpendicular components i_{11} decrease going from plane 1 to plane 2 and disappear in plane 3. On the other hand, the parallel components i_{12} do not appear in plane 1 and increase going from plane 2 to plane 3, because the TE mode wave has no component parallel to plane 1 and no component perpendicular to plane 3. On the z axis (i.e., at $\theta = 0°$ and 180°), the values of i_{11} in plane 1 coincide with those of i_{12} in plane 3 and the values of i_{11} and i_{12} in plane 2 agree with each other, as it must be. The cross components i_{12} have maxima at $\theta = 0°$ and

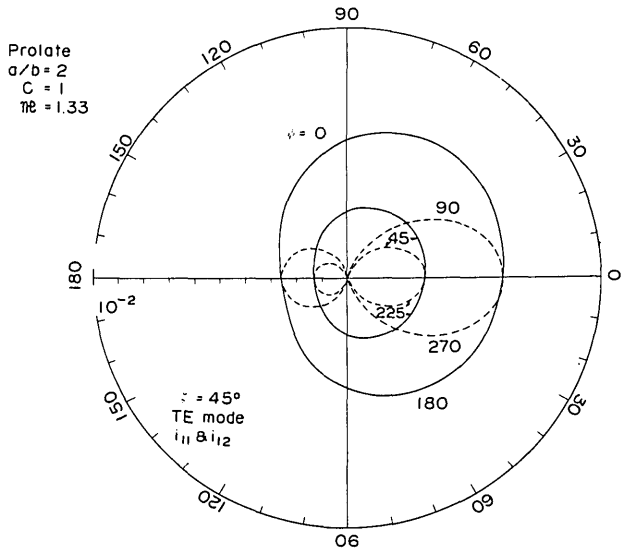

Fig. 6. Angular distribution of the intensity functions i_{11} (solid lines) and i_{12} (dashed lines) for the prolate spheroid of $c = 1$ and $a/b = 2$, and for $\zeta = 45°$. The figure shows, as a function of the zenith angle θ in the circular diagram, the distribution patterns in the three scattering planes through the z axis: one parallel to the incident plane ($\phi = 0°$ or 180°), one inclining from it by an angle 45° ($\phi = 45°$ or 225°), and one normal to it ($\phi = 90°$ or 270°).

180° and vanish at $\theta = 90°$, and their patterns are symmetric with respect to the rotation axis, while the components i_{11} show rather simple distribution patterns with θ, and i_{11} in plane 1 has a maximum at $\theta = 45°$ and $\phi = 0°$ (the forward direction) and a minimum near $\theta = 180°$, showing the predominated forward scattering and the asymmetric pattern with respect to the incident direction.

The corresponding distributions for $\zeta = 90°$ are displayed in Fig. 7. Compared with the case of $\zeta = 45°$, the backscattered intensities in plane 1 are enlarged, although the forwardly scattered intensities are hardly varied; it seems mainly due to the increment of the cross-sectional area of the spheroid normal to the incident direction [cf. Eq. (133)]. The angular distributions of both i_{11} and i_{12} are symmetric with respect to the incident direction.

In Figs. 8 and 9 are shown the intensity functions $i_{21}(\theta,\phi)$ and $i_{22}(\theta, \phi)$ for $\zeta = 45°$ and 90°, respectively, which correspond to the TM mode incident wave (case 2) for the same prolate spheroid. The components i_{22} polarized in the same mode to the incident light are given by solid lines and the cross-polarized components i_{21} by dashed lines in these figures. At $\zeta = 45°$ and 90°, the patterns for case 1 (Figs. 6 and 7) and case 2 (Figs. 8 and 9) are greatly different. The incident wave in case 2 has components both parallel and perpendicular to plane 3, which are proportional to $\sin\zeta$ and $\cos\zeta$, respectively, and naturally has no component normal to plane 1. As the incident angle ζ increases, the cross component i_{21} decreases and disappears at $\zeta = 90°$, while the component i_{22} increases, particularly in plane 3 and in the backward directions. For smaller angles ζ, however, the distribution patterns of i_{21} and i_{22} are similar, respectively, to those of i_{11} and i_{12}, because in the limit $\zeta \to 0$, i_{11} in plane 1 and i_{21} in plane 3 degenerate into the intensity function i_1 for the parallel incidence, and i_{12} in plane 3 and i_{22} in plane 1 into the function i_2.

Next, we shall briefly examine scattering by an oblate spheroid. Figure 10 illustrates the intensity functions i_{11} and i_{12} for the oblate spheroid of $c = 1$ and $a/b = 2$ for case 1 at $\zeta = 45°$. For case 2, the corresponding pictures are shown in Fig. 11. In these figures, the components polarized in the same mode as the incident wave (i_{11} and i_{22}) are given by solid

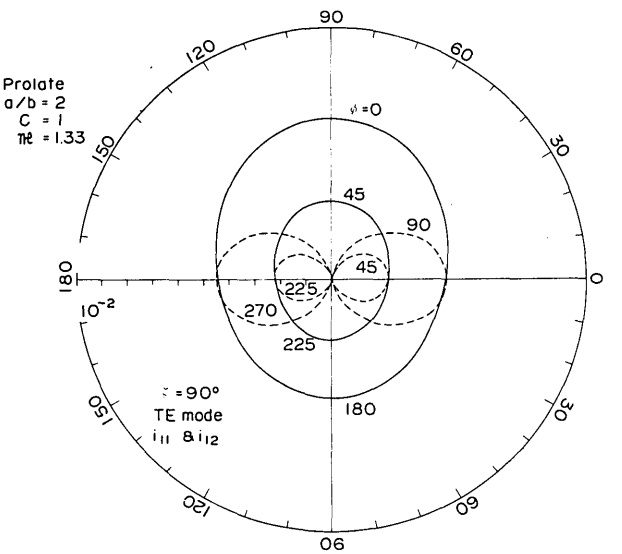

Fig. 7. Same as Fig. 6, but for $\zeta = 90°$.

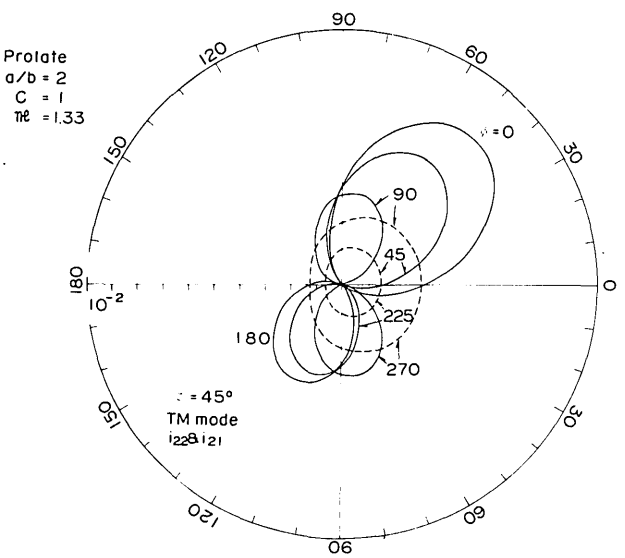

Fig. 8. Angular distribution of the intensity functions i_{22} (solid lines) and i_{21} (broken lines) for the prolate spheroid of $c = 1$, $a/b = 2$, and for $\zeta = 45°$ in the three azimuth planes.

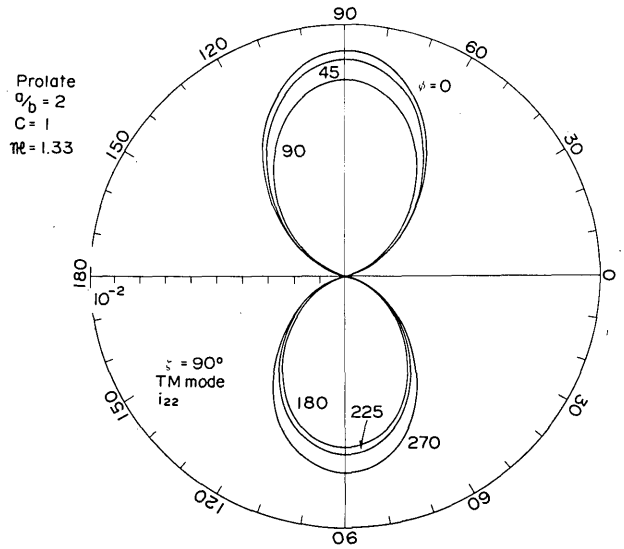

Fig. 9. Same as Fig. 8, but for $\zeta = 90°$.

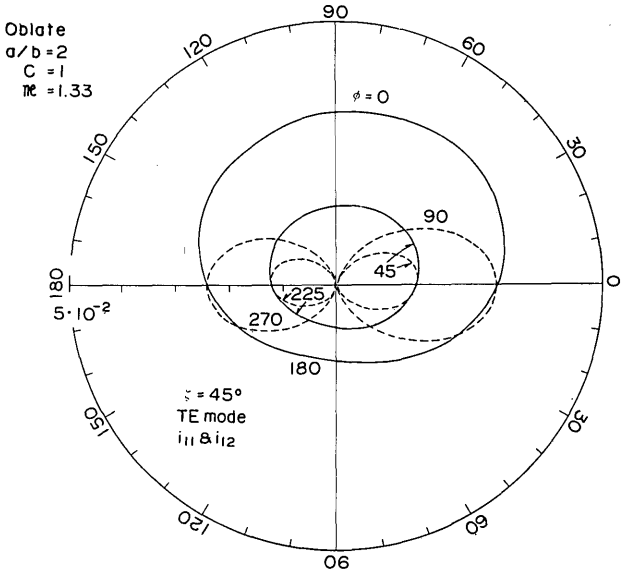

Fig. 10. Same as Fig. 6, but for the oblate spheroid of $c = 1$ and $a/b = 2$.

lines and the cross-polarized components i_{12} and i_{21} by dashed ones. In comparison with scattering by prolate spheroids, although the general patterns of the angular distribution of the intensity functions are similar to those for the prolate ones, some characteristic features can be seen from these figures. First, due to the fact that the volume of the oblate spheroid is larger than that of the prolate one with same values of c and a/b, the values of intensity functions for the oblate spheroid are larger than those for the prolate one. For the oblate spheroid, as ζ increases, all components decrease with one exception of i_{11} in plane 1 in the forward direction ($\theta = \zeta$); this feature is prominent, in particular, for case 2 and for the backward scattering, and it may be owing to the diminution of the cross-sectional area of the oblate spheroid with respect to the incident direction [cf. Eq. (134)].

C. Oblique Incidence of the Unpolarized Light

The Stokes parameters of the scattered light (I,Q,U,V) in the scattering plane can be expressed in terms of the Stokes parameters of the incident wave (I_0, Q_0, U_0, V_0) in the incident plane by means of the linear transformation (Ref. 11, p. 43–44); let $\mathbf{F}$ be the four-by-four transformation matrix, and let F_{ij} represent the elements in the ith row and jth column. For an unpolarized light with parameters (1,0,0,0), the scattered intensity and the degree of linear polarization are given by F_{11} and $-F_{21}/F_{11}$, respectively. To be explicit,

$$F_{11} \propto \frac{1}{2}(i_{11} + i_{12} + i_{21} + i_{22}), \qquad (130)$$

$$P = -\frac{F_{21}}{F_{11}} = \frac{(i_{11} + i_{21}) - (i_{12} + i_{22})}{(i_{11} + i_{21}) + (i_{12} + i_{22})}, \qquad (131)$$

where $1/2(i_{11} + i_{12} + i_{21} + i_{22})$ will be called the intensity functions for the unpolarized light at oblique incidence.

Figure 12 shows the angular distribution of the functions $1/2(i_{11} + i_{12} + i_{21} + i_{22})$ for the prolate spheroid of $c = 1$ and $a/b = 2$ at $\zeta = 45°$. The solid lines indicate the distribution in plane 1 ($\phi = 0°$ or 180°), the short broken ones in plane 2 ($\phi = 45°$ or 225°), and the long broken ones in plane 3 ($\phi = 90°$ or 270°). These curves can be, of course, drawn from Figs. 6 and 8. The patterns in the three azimuth planes are different, showing the effects of the shape; for such particles as spheres and spheroids at $\zeta = 0$, which are symmetric with respect to the unpolarized incident light, the scattered intensity is azimuthally symmetric. In plane 1, the scattered intensity takes a maximum in the forward directions ($\theta = 45°$) and

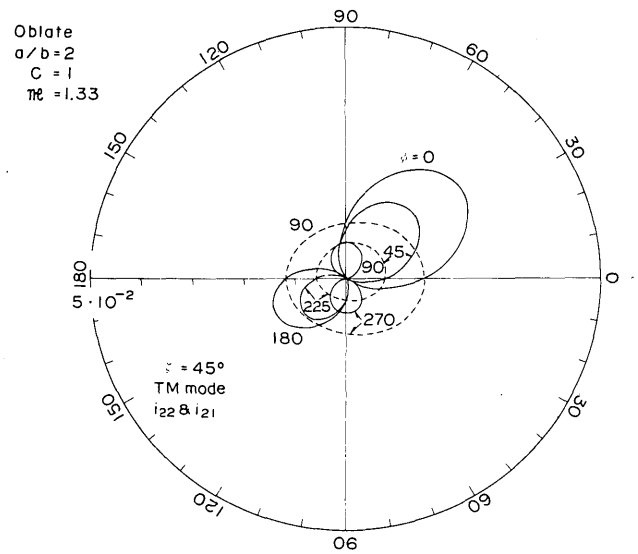

Fig. 11. Same as Fig. 8, but for the oblate spheroid of $c = 1$ and $a/b = 2$.

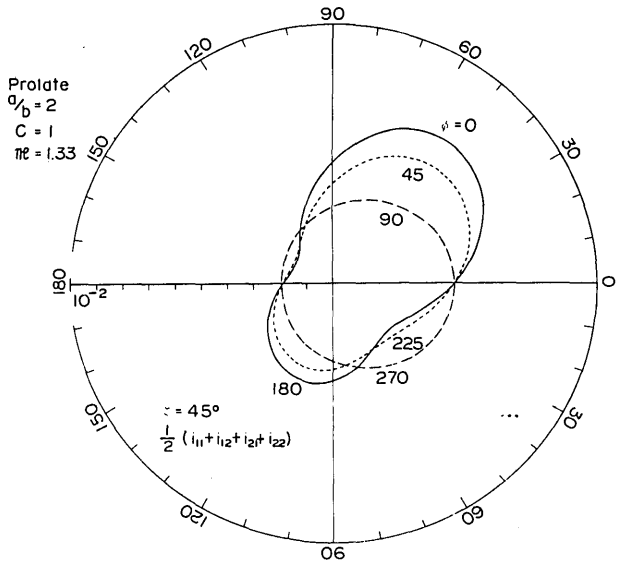

Fig. 12. Angular distribution of the intensity function $1/2(i_{11} + i_{12} + i_{21} + i_{22})$ for the prolate spheroid of $c = 1$ and $a/b = 2$, and for $\zeta = 45°$. The solid, short broken, and long broken lines indicate the distribution patterns in plane ($\phi = 0°$ or 180°), plane 2 ($\phi = 45°$ or 225°), and plane 3 ($\phi = 90°$ or 270°), respectively.

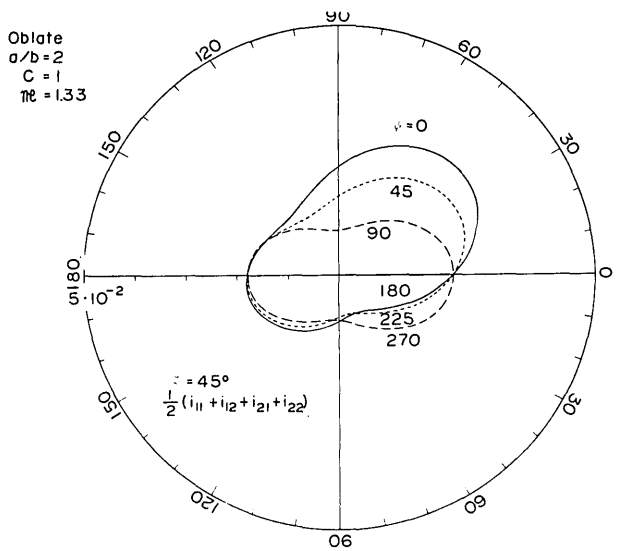

Fig. 13. Same as Fig. 12, but for the oblate spheroid of $c = 1$ and $a/b = 2$.

diminishes near the directions normal to the incident direction, while, in plane 3, the angular pattern shows a slight decrease of the intensity with increasing θ.

For the oblate spheroid of $c = 1$ and $a/b = 2$, the corresponding figure is given in Fig. 13. It is characteristic that the intensity in plane 3 becomes minimum in the direction $\theta = 90°$, and it is due to no contribution of i_{12} to the direction as shown in Fig. 10.

For larger spheroids, the distribution patterns become much complicated with great fluctuations with θ and ϕ. Figure 14 illustrates the logarithmic values of the intensity functions $1/2(i_{11} + i_{12} + i_{21} + i_{22})$ for the prolate spheroid of $c = 5$ and $a/b = 2$ at $\zeta = 45°$, as a function of the zenith angle θ measured from the positive z axis. The solid, short broken, and long broken lines give, respectively, the values in plane 1, plane 2, and plane 3. The angular distribution in plane 1 shows the asymmetric pattern with respect to the incident direction and the strong forward scattering peak in absence of a peak in the backward direction. The latter peak is a characteristic of transparent particles with symmetric form to the incident direction. In plane 3, the scattered intensity takes a maximum at $\theta = 0°$ and minima in the directions $\theta \approx 160°$, and is symmetric with respect to the z axis (the axis of revolution).

The corresponding figure for $\zeta = 90°$ is given in Fig. 15. The distribution patterns are naturally symmetric with respect to the incident direction.

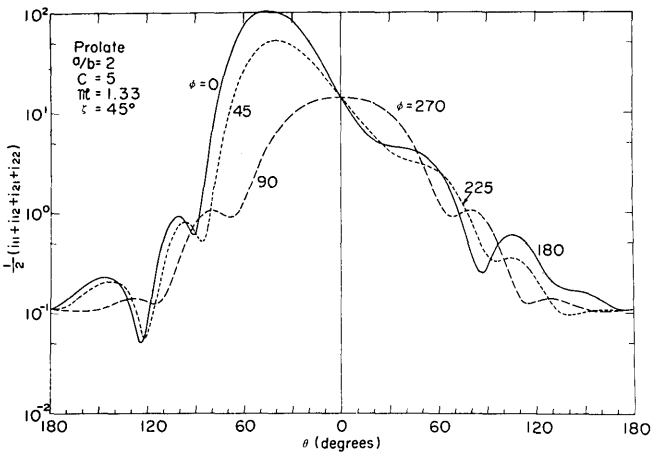

Fig. 14. Angular distribution of the intensity function $1/2(i_{11} + i_{12} + i_{21} + i_{22})$ for the prolate spheroid of $c = 5$ and $a/b = 2$, and $\zeta = 45°$. The solid, short broken, and long broken lines give logarithmic values in plane 1, plane 2, and plane 3, respectively, as a function of θ.

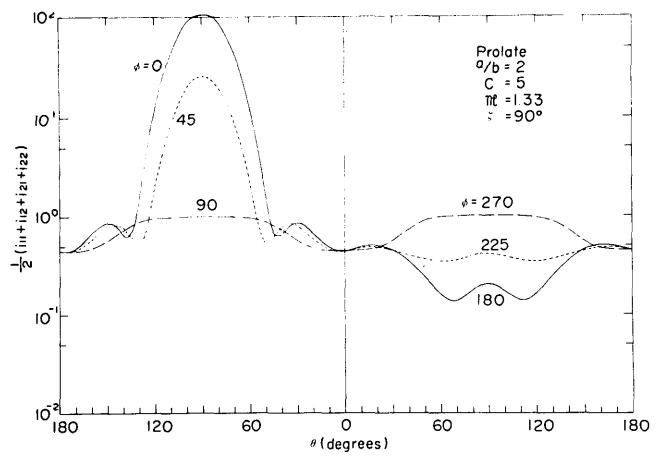

Fig. 15. Same as Fig. 14 but for $\zeta = 90°$.

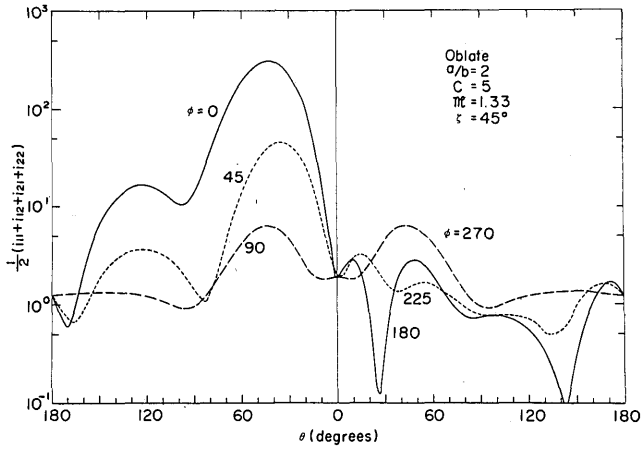

Fig. 16. Same as Fig. 14, but for the oblate spheroid of $c = 5$ and $a/b = 2$.

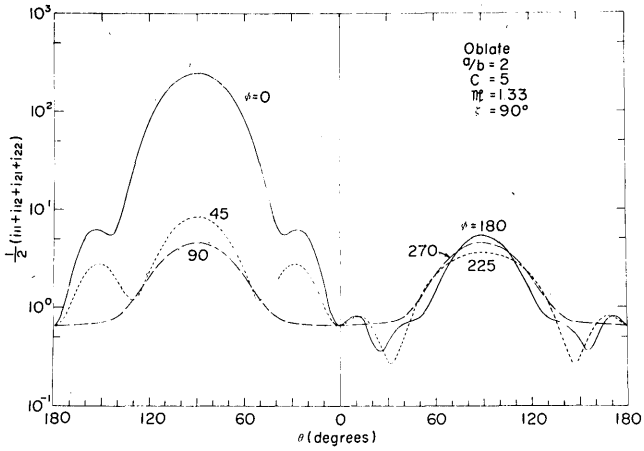

Fig. 17. Same as Fig. 15, but for the oblate spheroid of $c = 5$ and $a/b = 2$.

Figures 16 and 17 show the distributions for the oblate spheroid of $c = 5$ and $a/b = 2$ at oblique incidences of $\zeta = 45°$ and 90°, respectively. For $\zeta = 45°$, the intensity functions in plane 1, fluctuate greatly, showing a broad second maximum around $\theta = 130°$ in $\phi = 0°$ and deep minima near $\theta = 25°$ and 145° in $\phi = 180°$. The intensities in plane 3 have maxima at $\theta = 45°$ rather than at $\theta = 0°$ and 180° in the case of the small oblate spheroid (Fig. 13). For this large oblate spheroid, contribution to the backward scattering increases at the large incident angle $\zeta = 90°$ because of the symmetrical orientation to the incident light, although the cross-sectional area decreases.

XI. Scattering Cross Sections and Efficiency Factors

The scattering efficiency factor Q_{sca} is here defined by the ratio of the scattering cross section C_{sca} to the area of the geometrical cross section of the spheroid, normal to the incident direction, at the center. Thus,

$$Q_{sca} = C_{sca}/G(\zeta), \tag{132}$$

where $G(\zeta)$ is the cross-sectional area of the spheroid at the incident angle ζ and is given by

$$G(\zeta) = \frac{\pi a b^2}{(a^2 \cdot \cos^2\zeta + b^2 \cdot \sin^2\zeta)^{1/2}} \tag{133}$$

for the prolate spheroid and

$$G(\zeta) = \frac{\pi a^2 b}{(b^2 \cdot \cos^2\zeta + a^2 \cdot \sin^2\zeta)^{1/2}}, \tag{134}$$

for the oblate one,[14] which become, respectively, πb^2 and πa^2 for $\zeta = 0°$, and both of which are πab for $\zeta = 90°$; the sectional area of the prolate spheroid increases monotonously with increasing incident angle ζ, while that of the oblate spheroid decreases.

Figure 18 shows the scattering efficiency factors Q_{sca} at the parallel incidence ($\zeta = 0°$) as a function of the size parameter c. The efficiency factors for the prolate spheroids of $a/b = 2$, 5, and 10 are given by solid lines and those for the oblate spheroids of $a/b = 2$ by a long broken line. As a reference, the efficiency factors for homogeneous spheres computed by using the Mie theory are also drawn by a short broken line, and, for this curve, the values of the abscissa should

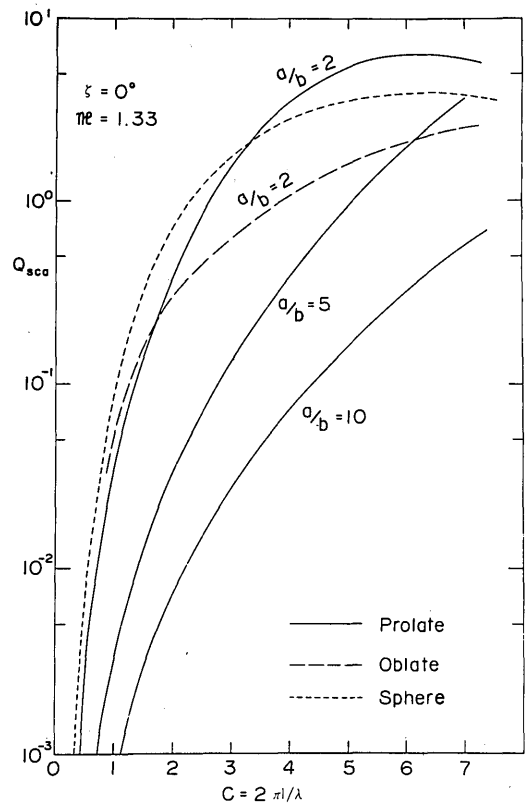

Fig. 18. Scattering efficiency factors Q_{sca} at $\zeta = 0°$ as a function of the size parameter c for the prolate spheroids of $a/b = 2$, 5, and 10 (solid lines) and for the oblate spheroid of $a/b = 2$ (long broken lines). The curve for the sphere is also shown by a short broken line.

be read as values of the size parameter of the Mie theory. In this size range, the efficiency factors of the prolate spheroids increase as c increases, and at a given size, they are smaller for larger a/b. The pattern for the prolate spheroids of $a/b = 2$ is very similar to that for spheres showing an initial maximum in the so-called resonance region, i.e., $Q_{sca} = 6.5$ at $c = 6$. Greenberg *et al.*[15] have obtained the numerical results on the efficiency factors of the prolate spheroids up to elongations of two, for the scalar wave propagated along the axis of the spheroid (i.e., $\zeta = 0°$) by the point-matching technique, which is a method approximating the boundary conditions at finite number of points on the boundary. A noteworthy aspect of their results is the increasing height of the first broad maximum in the efficiency curves with increasing elongation of the spheroid as well as a deeper dip in the first minimum. This effect is also observed in our results. In addition, it is interesting that the scattering efficiency computed by them for the spheroid of $a/b = 2$ and $\mathfrak{N} = 1.3$ has the maximum value of about 6 at the phase shift $2kb|\mathfrak{N} - 1| = 2$ or, with our size parameter, at $c = 5.8$, showing a good agreement with our results by the rigorous solution.

For the oblique incidence of $\zeta = 45°$ and 90°, the scattering efficiency factors of the prolate spheroid with $a/b = 2$ are given in Fig. 19 by solid lines for case 1 (TE mode) and by long broken lines for case 2 (TM mode). The curve for $\zeta = 0°$, which is already drawn in Fig. 18, is given by short broken lines. The scattering cross section $C_{1,sca}$ for case 1 and $C_{2,sca}$ for case 2 at oblique incidence were computed by Eq. (116) and (118), respectively. As $\zeta \to 0$, both $Q_{1,sca}$ and $Q_{2,sca}$ tend to Q_{sca} for the parallel incidence.

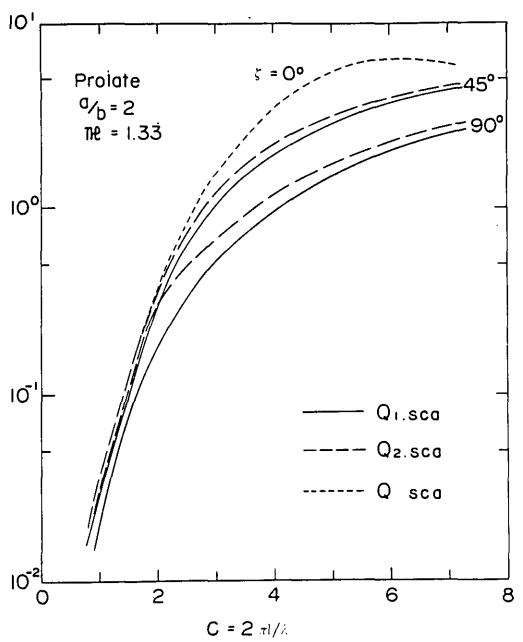

Fig. 19. Scattering efficiency factors $Q_{1,sca}$ (solid lines) and $Q_{2,sca}$ (long broken lines) as a function of c for the prolate spheroid of $a/b = 2$ and for $\zeta = 45°$ and 90°. Curve for $\zeta = 0°$, or Q_{sca}, is also shown by a short broken line.

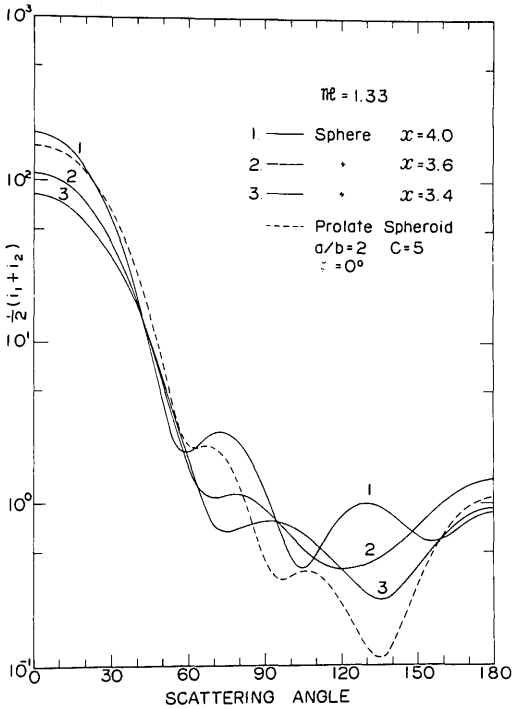

Fig. 20. Angular distribution of the intensity function $1/2(i_1 + i_2)$ for the prolate spheroid of $c = 5$ and $a/b = 2$ (dashed line) and for the spheres of the size parameter $x = 4.0$, 3.6, and 3.4 (solid lines).

For the small spheroids of $c \lesssim 7$, the efficiency factors are smaller for larger incident angle ζ, and for a given angle ζ, $Q_{2,sca}$ is larger than $Q_{1,sca}$; the differences of $Q_{2,sca}$ and $Q_{1,sca}$ increase as ζ increases. This result is supported by the experimental results[15,16] on the extinction cross section of the microwave for an arbitrarily oriented prolate spheroid with $2\pi b/\lambda = 2.5$, $\mathfrak{N} = 1.25$, and $a/b = 2$. For an unpolarized incident light, the scattering efficiency factors are given by $1/2(Q_{1,sca} + Q_{2,sca})$

Finally, an example of comparison of the scattering by a spheroid with that by a sphere is displayed. In Fig. 20, the angular distributions of the intensity function $1/2(i_1 + i_2)$ for unpolarized incident light are shown for the prolate spheroid of $c = 5$, $a/b = 2$ at $\zeta = 0°$ by dashed curves and for spheres with size parameters $x = 4.0$, 3.6, and 3.4 by solid curves. The values of $x = 3.6$ and 4.0 are chosen so that the spheres have the same volume as that of the spheroid and the cross-sectional area is equal to the area of the ellipse πab; the size parameter of the sphere giving the area equal to the sectional area πb^2 of the spheroid is $x = 2.9$. The angular patterns of the spheroid in the forward region are very similar to those for spheres, but they are different at scattering angles greater than 60°. The intensities scattered by the spheroid are nearest to those of the largest sphere ($x = 4.0$) in the forward region and to those of the smallest one ($x = 3.4$) in the backward region. The value of $(4\pi/\lambda^2)C_{sca}$ of this spheroid is nearly equal to that of the sphere with $x = 4.0$; the total radiation

scattered by the spheroid is, in this case, of same magnitude as that by the sphere having the equivalent area to πab, rather than the volume equal to that of the spheroid.

This work was supported partly by the Ministry of Education of Japan under Fund for Scientific Research C 754057 and partly by the U.S. National Environmental Satellite Service under Contract 2-37151.

References

1. G. Mie, Ann. Phys. **25,** 377 (1908).
2. Lord Rayleigh, Phil. Mag. **36,** 365 (1918).
3. J. R. Wait, Can. J. Phys. **33,** 189 (1955).
4. F. Möglich, Ann. Phys. **83,** 609 (1927).
5. F. V. Schultz, "Scattering by a Prolate Spheroid," UMM-42, Univ. of Mich., 1950.
6. K. M. Siegel, F. V. Schultz, B. H. Gere, and F. B. Sleator, IRE Trans. Antennas Propag. **AP-4,** 266 (1956).
7. J. A. Stratton, *Electromagnetic Theory* (McGraw-Hill, New York, 1941).
8. M. Born and E. Wolf, *Principles of Optics* (Pergamon Press, Oxford, 1970).
9. C. Flammer, *Spheroidal Wave Functions* (Stanford U.P., Stanford, Calif., 1957).
10. J. R. Wait, Radio Sci. **1,** 475 (1966).
11. H. C. van de Hulst, *Light Scattering by Small Particles* (Wiley, New York, 1957).
12. C. W. H. Yeh, J. Math. Phys. **42,** 68 (1963).
13. C. J. Bouwkamp, J. Math. Phys. **26,** 79 (1947).
14. R. J. T. Bell, *Coordinate Solid Geometry* (Macmillan, London, 1948).
15. J. M. Greenberg, A. C. Lind, R. T. Wang, and L. F. Libelo, in *Electromagnetic Scattering,* R. L. Rowell and R. S. Stein, Eds. (Gordon and Breach, New York, 1967).
16. A. C. Lind, R. T. Wang, and J. M. Greenberg, Appl. Opt. **4,** 1555 (1965).

OSA Instructions for Post-Deadline Papers

The Executive Committee of the Board of Directors, at its meeting on 9 December 1970, instituted a new policy toward presentation of post-deadline papers at the semiannual meetings of the Society. In order to give participants at the meetings an opportunity to hear new and significant material in rapidly advancing areas of optics, authors will be provided with the opportunity to present results that have been obtained after the normal deadline for contributed papers. The regulations that govern the submission of post-deadline papers follow:

(1) In order to be considered for the post-deadline session(s) an author must submit a 1000-word summary in addition to the information required on the standard abstract form. The 1000-word abstract will be used in selecting papers to be accepted. The 200-word abstracts of accepted papers will be published in the Journal of the Optical Society of America.

(2) Post-deadline papers are to be submitted to the Executive Director, Optical Society of America, 2100 Pennsylvania Avenue, N.W., Washington, D.C. 20037. Only those received by the Thursday preceding an OSA meeting can be duplicated and distributed in time for the program committee meeting.

(3) The program committee for the selection of post-deadline papers consists of the Technical Council, the Executive Director, and any others designated by the chairman of the Technical Council. This group will meet before the first full day of the OSA meeting. The chairman of the Technical Council, or someone designated by him, will preside.

(4) Only post-deadline papers judged by the appropriate members of the program committee to be truly excellent and compelling in their timeliness will be accepted.

(5) The accepted post-deadline papers will be placed at the end of related sessions of contributed papers, if possible, or in a separate session if necessary. The number of papers accepted will be governed by the time available as well as by the requirements of Regulation (4).

(6) Multiple papers by the same author will be handled in a manner consistent with OSA policy. Accepted post-deadline papers will have priority over multiple papers by the same author that are scheduled in the same session.

(7) After post-deadline papers have been selected, a schedule will be printed and made available to the attendees early in the meeting. Copies of the 200-word abstracts will also be available.

(8) The 200-word abstracts will be printed in the Journal in due course. They will not appear with the regular program but at a later date as the printing schedule permits.

(9) The selection and scheduling of post-deadline papers will be done with the interests of the attendees given principal consideration.